Identification of Circular RNAs Regulating Cardiomyocyte Proliferation in Neonatal Pig Hearts

Ling Tang,[1,*] Verah Nyarige,[1,2,*] Pengsheng Li,[1] Junwen Wang,[2,3,#] Wuqiang Zhu,[1,#]

[1]Department of Cardiovascular Medicine, Physiology and Biomedical Engineering, Center for Regenerative Biotherapeutics, Mayo Clinic Arizona, Scottsdale, AZ, USA

[2]Department of Quantitative Health Sciences Research, Center for Individualized Medicine, Mayo Clinic Arizona, Scottsdale, AZ, USA

[3]Division of Applied Oral Sciences & Community Dental Care, Faculty of Dentistry, The University of Hong Kong, Hong Kong SAR, China

*These authors contribute to the work equally

ABSTRACT

Little is known about the expression patterns and functions of circular RNAs (circRNAs) in the heart of large mammals. In this study, we examined the expression profiles of circRNAs, microRNAs (miRNAs), and messenger RNAs (mRNAs) in neonatal pig hearts. Pig heart samples collected on postnatal days 1 (P1), 3 (P3), 7 (P7) and 28 (P28) were sent for total RNA sequencing. Our data revealed a total of 7000 circRNAs in the 24 pig hearts. Pathway enrichment analysis of hallmark gene sets demonstrated that differentially expressed circRNAs are engaged in different pathways. The most significant difference was observed between P1 and the other three groups (P3, P7 and P28) in pathways related to cell cycle and muscle development. Out of the ten circRNAs that were validated through real-time quantitative polymerase chain reaction (qRT-PCR) to confirm their expression, six exhibited significant effects on cell cycle activity in human induced pluripotent stem cells-derived cardiomyocytes (hiPSC-CMs) following small interfering RNA-mediated knockdown. The circRNA-miRNA-mRNA networks were constructed to understand the potential mechanisms of circRNAs in the heart. In conclusion, our study provided a dataset for exploring the roles of circRNAs in pig hearts. In addition, we identified several circRNAs that regulate cardiomyocyte cell cycle.

Introduction

Heart failure continues to be a major cause of death worldwide. The primary reason for heart failure is the degeneration or loss of functional cardiomyocytes after injury. It is well established that cardiomyocytes in adult mammals possess limited regenerative potential as a result of cell cycle exit. Therefore, myocardium loss after myocardial injuries is typically replaced by fibrotic scar. Thus, replenishing lost cardiomyocytes emerges as a promising strategy for repairing damaged myocardium and improving heart function in preclinical models of heart failure. It was reported that the heart of neonatal mice retains regenerative capacity within the first week after birth which is mediated by proliferation of endogenous cardiomyocytes (1). Several cell types and pathways are involved in cardiomyocyte proliferation, which includes hormones, revascularization, nerve signaling, immune response, extracellular matrix, metabolism, and gene expressions, et al (2). We have recently shown that neonatal pigs can also regenerate lost myocardium in the first two days after birth in response to myocardial injuries (3). Specifically, hearts of postnatal day one pigs hold robust regeneration capacity following myocardial infarction. This regeneration is mediated by the proliferation of preexisting cardiomyocytes, which is lost when cardiomyocytes permanently exit the cell cycle. Thus far, molecular mechanisms underlying the injury-induced activation of cardiomyocyte cell cycle in neonatal pig hearts remains largely unknown.

Circular RNA (circRNA) is a type of RNA molecule that forms a closed loop structure. circRNAs are divided into four categories: ecRNAs (exonic circRNAs) which are derived

from single or multiple exons, ciRNAs (circular intronic RNAs) which are derived from introns, EIciRNAs (exon-intron circRNAs) which are composed of exons and introns, and tricRNAs (tRNA intronic circRNAs) which are formed by splicing tRNA introns (4). Previous studies have reported consistent expression of circRNAs in various human tissues and bodily fluids, including blood, saliva, and urine (5-7). circRNAs play an important role in regulating various biological processes. The unique closed loop structure renders them resistant to degradation by ribonucleases and ensures stability. This stability allows circRNAs to accumulate in cells, making them potential biomarkers for various cardiovascular conditions. circRNAs carry out their functions through mechanisms related to transcription regulation, such as miRNA sponging, formation of RNA-protein complexes, and interactions with RNA-binding proteins (RBPs) (4, 8). circRNAs can act as microRNA sponges, binding to and sequestering miRNAs, thus preventing them from binding to their target mRNAs and suppressing gene expression. Additionally, circRNAs are well-known for their specificity to certain tissues and developmental stages (8).

Recent studies highlighted the importance of circRNAs in the regulation of cardiovascular functions (9). The involvement of circRNAs in regulating cardiomyocyte proliferation and heart regeneration has only been established for a few circRNAs, including circNfix (10), circHipk3 (11), circCDYL (12), and circMdc1 (13). However, more research has been done to identify new circRNAs that are involved in regulating the pathophysiology of the diseased heart, such as cardiac inflammation (14-16), apoptosis (17-32), autophagy (33-35), ferroptosis (36), angiogenesis (37, 38), fibrosis (39), and modulating the expression

and/or activity of these circRNAs has been shown to provide cardioprotection following myocardial injuries.

Despite these encouraging results, majority of these studies were performed on rodents. The expression patterns and function of circRNAs in the hearts of large animals are essentially unknown. The main objective of this study is to fill this knowledge gap by examining the expression profiles and functions of circRNAs in neonatal pig hearts. We were particularly interested in identifying the circRNAs that regulate cardiomyocyte cell cycle and proliferation. Toward this goal, we performed total RNA sequencing with pig heart samples collected on postnatal days 1 (P1), 3 (P3), 7 (P7) and 28 (P28), and analyzed the expression profiles of circRNAs, miRNAs, and mRNAs. Our data revealed significant changes in the expression of circRNAs at different postnatal stages (i.e., from postnatal day 1 to day 28), and pathway enrichment analysis highlighted circRNAs that are associated with cell division and proliferation. Functional analysis confirmed the cell cycle function of six new circRNAs in cardiomyocyte. By predicting interactions between circRNAs, miRNAs, and mRNAs, we were able to infer potential relationships and construct an integrated regulatory network. This comprehensive analysis provided insights into the complex regulatory processes involving circRNAs, miRNAs, and mRNAs during postnatal heart development in newborn pigs. Additionally, our study generated a dataset for further exploration of circRNA roles in the heart of neonatal pigs.

Results

We performed RNA sequencing of mRNAs and noncoding RNAs including circRNAs and miRNAs using samples from neonatal pig hearts at different developmental stages (P1, P3, P7, and P28; with 6 animals at each age). The heart samples were sent to two different companies for sequencing (Supplemental table 1). In the first batch, 12 samples from animals of different ages (3 animals at each age) were sent to Novogene Inc. for circRNA sequencing (annotated as “nv1”). A second batch of 12 more samples was sent to CD Genomocs Inc. (annotated as “cd”) for total RNA sequencing. In the third batch, new samples from the same 12 animals in the first batch were sent to Novogene Inc. (annotated as “nv2”) for total RNA sequencing again. We validated the sequencing data using real-time quantitative polymerase chain reaction (qRT-PCR), performed differential expression analysis and pathway enrichment analysis using different bioinformatics tools, and conducted functional experiments in the cultured cardiomyocytes via small interfering RNA (siRNA) mediated knockdown of selected circRNA candidates. Schematics of experimental design were shown in Supplemental Figure 1.

Differentially expression analysis of circRNAs in neonatal pig hearts. We analyzed circRNA expression profiles in neonatal pig hearts using circRNA sequencing data from all three batches (nv1, cd, and nv2; 36 samples) which covered a total of ~7000 circRNAs. A principal component analysis (PCA) of our batch corrected samples exhibited a great random mixing of samples from the three batches, implying successful cross-sample batch correction. The most noteworthy difference was observed between P1 and the other three groups. Although samples within the other groups exhibited closer similarities to one another, there were occasional individual samples that displayed similarities to

samples from different groups. This occurrence is likely due to the deliberate selection of samples from neonatal pigs to detect subtle differences in their cardiac regenerative function. Therefore, the experimental design remains reasonable, and the biological replications are considered satisfactory (Supplemental Figure 2A).

Differentially expressed (i.e., upregulated or downregulated) circRNAs were identified from various comparisons (i.e., P1 versus P3, P1 versus P7, P1 versus P28, and P1 versus P3, P7 and P28, Supplemental Figure 2B) and the highest number of differentially expressed circRNAs was observed in the comparison between P1 and P28. Volcano plots were generated to provide a comprehensive view of the differential expression patterns (Supplemental Figure 2C-2F). To understand potential involvement of circRNA host genes in cell cycle regulation, circRNA that were enriched in cell cycle related pathways were identified and utilized to generate heatmaps. These heatmaps displayed the expression patterns of the differentially expressed and top ranked cell cycle related circRNAs across different ages (Figure 1A-1D). Pathway enrichment analysis of the hallmark gene sets from the Human Molecular Signatures Database (MSigDB) (40) demonstrated that differentially expressed circRNAs were enriched in different pathways associated with cell cycle activities, such as mitotic spindle assembly and myogenesis, cell cycle checkpoint, and the E2F- or Myc-target genes (P1 versus P3, Figure 1E; P1 versus P7, Figure 1F; P1 versus P28, Figure 1G; and P1 versus P3, P7, and P28, Figure 1H). The leading edge genes associated with these pathways were listed in Supplemental table 2. These findings demonstrated significant changes in pathways related to cell division, mitotic spindle assembly, skeletal muscle development, and protein secretion

due to differential circRNA expression. Taken together, this data provided detailed information about circRNA expression profiles in neonatal pig hearts, indicating their potential involvement in heart development.

Time-varying effect modeling (TVEM) of cell cycle regulating circRNAs. A notable advantage of the current study is that we examined the expression profile of circRNA in pig hearts at different postnatal ages. To evaluate the overall time dependency of circRNA expression in cell cycle related functions, we utilized our circRNA dataset to analyze how the expression of different cell cycle enriched sets of circRNA host genes varied across different postnatal days. This was achieved by TVEM analysis of the host genes described above. For each of the selected cell cycle related pathways, we then reported and visualized the changes in the β_1 coefficient across different postnatal periods (Supplemental Figure 3). We observed significant variation in the β_1 coefficients over time in core cell cycle related pathways such as G2M checkpoint (Supplemental Figure 3A), mitotic spindle (Supplemental Figure 3B), Myc-targets (Supplemental Figure 3C-3D), myogenesis (Supplemental Figure 3E), PI3K-Akt-mTOR signaling (Supplemental Figure 3F), and Wnt-beta catenin signaling (Supplemental Figure 3G), suggesting that circRNAs potentially play a crucial role in regulating cell cycle during postnatal heart development.

Differential expression analysis of miRNAs and mRNAs in neonatal pig hearts. We did not have a good batch correction for miRNA sequencing data from batches “cd” and “nv2”. Therefore, we analyzed the expression profiles of miRNAs and mRNAs using data from batch “cd” only. The PCA plots of sequencing data for miRNA (Supplemental Figure 4A)

and mRNA (Supplemental Figure 5A) showed clear distinctions among the four groups. The number of differential expressed miRNAs in various comparisons (i.e., P1 versus P3, P1 versus P7, P1 versus P28, and P1 versus P3, P7 and P28) was provide for miRNA (Supplemental Figure 4B) and mRNA (Supplemental Figure 5B), and the highest number of differentially expressed miRNAs and mRNAs was observed in the comparison between P1 and P28. Volcano plots were generated to present a complete overview of the differential expression profiles for miRNAs (Supplemental Figure 4C-4F) and mRNAs (Supplemental Figure 5C-5F). Heatmaps were generated to display the expression patterns for the top ranked, differentially expressed miRNAs (Figure 2A-2D) and mRNAs (Figure 3A-3D) associated with cell cycle. This highlighted the levels of intensity across various samples and showed the time dependency in the expression of these RNAs. The pathway analyses of mRNA data resulted to enrichment of various pathways, such as inflammation, responses to hypoxia, epithelial-mesenchymal transition, oxidative phosphorylation, mTORC1 related genes, and cell cycle targeted genes (P1 versus P3, Figure 3E; P1 versus P7, Figure 3F; P1 versus P28, Figure 3G; and P1 versus P3, 7, and 28, Figure 3H). The resulted top leading edge associated with these pathways were listed in Supplemental table 3. As it can be inferred from the information above, a notable difference in the comparison between P1 and other groups is the presence of pathways that are associated with cell cycle and metabolism (Figure 3E-3H).

Validation of circRNA expression in neonatal pig hearts. We validated the expression of top-ranked, differentially expressed circRNAs in cell cycle related pathways from the RNA sequencing using qRT-PCR on different ages of pig heart samples. Ten circRNAs

showed consistent results between qRT-PCR and circRNA sequencing across all time points (P1, P3, P7, and P28), including sus-ABLIM1_0001, sus-RNF13_0002, sus-KIF1B_0001, sus-MYOM1_0001, sus-AGL_0001, sus-PDLIM5_0001, sus-CDH13_0001, sus-CDC42_0001, sus-TBCD_0003, and sus-ENSSSCG00000026041_0001 (Figure 4A-4J). Expression of some circRNAs were initially increased and then decreased as the pigs matured, such as sus- sus-RNF13_0002 (Figure 4B), sus-KIF1B_0001 (Figure 4C), sus-MYOM1_0001 (Figure 4D), sus-PDLIM5_0001 (Figure 4F), sus-CDH13_0001 (Figure 4G), sus-CDC42_0001 (Figure 4H), sus-TBCD_0003 (Figure 4I), and sus-ENSSSCG00000026041_0001 (Figure 4J). However, some circRNAs did not show a consistent expression pattern aligned with cardiomyocyte maturation, such as sus-ABLIM1_0001 (Figure 4A) and sus-AGL_0001 (Figure 4E). We used the circAtlas(v2) database to match pig circRNAs to their corresponding pig chromosomes, except for sus-ENSSSCG00000026041_0001 for which we could not find matched sequence in this database. The validated circRNA information obtained from the circAtlas(v2) database is listed in Supplemental table 4. The results obtained from qRT-PCR, which measures expression levels, were consistent with the patterns observed in RNA sequencing. This confirms the accuracy of our findings.

circRNAs that regulate cell cycle. We conducted a phenotypic validation of the functions of the nine circRNAs (Supplemental table 4, except for sus-ENSSSCG00000026041_0001 which we could not find matched sequence in the database) using human induced pluripotent stem cells-derived cardiomyocytes (hiPSC-CMs) as there are no appropriate pig cardiomyocyte lines available. To accomplish this,

we initially matched pig circRNAs to their respective human circRNAs using the circAtlas(v2) database. We successfully matched six pig circRNAs with human circRNAs, namely hsa-ABLIM1_0001, hsa-RNF13_0004, hsa-KIF1B_0001, hsa-MYOM1_0001, hsa-AC096949_0001 and hsa-PDLIM5_0001 (Supplemental table 5). We then assessed the impact of siRNA-based knocking down of these six circRNAs on the cell cycle of hiPSC-CMs (Figure 5-7). These cells carry a luciferase gene, allowing us to estimate the cell number through a bioluminescence assay as previously described (41-43). Our data showed that reducing the expression of hsa-ABLIM1_0001 (Figure 5A), hsa-RNF13_0004 (Figure 5C) and hsa-KIF1B_0001 (Figure 5E) resulted in an increased cell cycle activity, as demonstrated by a 2-3 fold rise of fluorescence intensity in the bioluminescence assays (Figure 5B, 5D, and 5F, respectively), along with a 3-4 fold rise in the proportion of hiPSC-CMs positively stained with Bromodeoxyuridine (BrdU, a S phase maker) and PH3 (a M phase marker), compared to cells in the control group (Figure 6A-6B, and 7A-7B, respectively). Conversely, inhibiting the expression of hsa-MYOM1_0001 (Figure 5G), hsa-AC096949_0001 (Figure 5I) and hsa-PDLIM5_0001 (Figure 5K) resulted in decreased cell cycle activity as shown by a 50% of reduction in fluorescence intensity in the bioluminescence assays (Figure 5H, 5J, and 5L, respectively), and a 50-70% decrease in the proportion of BrdU- and PH3-positively stained hiPSC-CMs compared to cells in control group (Figure 6A-6B, and 7A-7B, respectively). It was reported that mature miRNAs and mRNAs primarily function in the cytoplasm (44), and circRNAs regulate gene expression by binding to miRNAs (4). In our study, we examined the intracellular localization of six circRNAs that we have shown to regulate the cell cycle. Our data demonstrated that all these circRNAs were

predominantly located in the cytoplasm, particularly in the peri-nuclei region, with some also present in the nuclei of hiPSC-CMs (Supplemental Figure 6A-6F).

circRNA-miRNA-mRNA network construction

To better understand the potential molecular mechanism of circRNAs involved in the process of cell proliferation, circRNAs and their predicted targets at different stages of heart development were used to construct a circRNA-miRNA-mRNA regulatory network (Supplemental Figure 7A-7C). Specifically, we selected five pig circRNAs that were conserved in human, including sus-ABLIM1_0001, sus-RNF13_0002, sus-KIF1B_0001, sus-AGL_0001, and CDH13_0001. Using circAtlas(v2), we predicted a total of 11 target miRNAs. A total of 45 target mRNAs for the 11 miRNAs were then predicted using miRNAtap (45) package in R. To infer potential circRNA-miRNA-mRNA relationships, we used Cytoscape software was used to generate circRNA-miRNA-mRNA networks (46). These RNA interactions provide new insights into the potential mechanism for cell proliferation. Specifically, we predicted interactions such as sus-ABLIM1_0001 with miR-31-5p, miR-105-3p, miR-197-3p, miR-214-5p, miR-215-3p (Supplemental Figure 7A-7C) and miR-105-3P (Supplemental Figure 7C), sus-KIF1B_0001 with miR-140-5p, miR-18a-3p and miR-15a-3p (Supplemental Figure 7A-7C), sus-RNF13_0002 with miR-7-5p (Supplemental Figure 7A-7C), sus-CDH13_0001 with miR-132-5p (Supplemental Figure 7A-7C), and sus-AGL_0001 with miR-128-3p (Supplemental Figure 7C). To validate these predictions and determine if circRNAs regulate the expression of these miRNAs, we treated hiPSC-CMs with siRNAs targeting the circRNAs. We then examined the impact of circRNA knockdown on the expression levels of the predicted miRNAs. Our

data showed that, compared to hiPSC-CMs treated with a control siRNA, those treated with has-ABLIM1_0001 siRNA showed a significant increase of miR-31-5p, miR-197-3p, and miR-215-3p, while the expression levels of miR-214-5p and miR-105-3p remained unchanged (Figure 8A). Additionally, hiPSC-CMs treated with has-KIF1B_0001 siRNA exhibited a significant decrease of miR-140-5p and miR-15a-3p compared to the control (Figure 8B). On the other hand, hiPSC-CMs treated with hsa-AC096949_0001 (the human counterpart of pig circRNA sus-AGL_0001) siRNA displayed a significant increase of miR-128-3p compared to the control (Figure 8C). Unfortunately, we were not able to detect miR-7-5p after the transfection of siRNAs targeting the circRNA RNF13_0002. In addition, the siRNAs for circRNA has-CDH13_0001 did not work for unknown reasons (data not shown).

To determine if modulating the expression of these miRNAs alters cardiomyocyte cell cycle, hiPSC-CMs were treated with miRNA siRNAs or mimics, respectively. Bioluminescence assays were used to estimate the number of hiPSC-CMs. Our data indicated that inhibiting miR-31-5p, miR-197-3p, or miR-215-3p using different concentrations of miRNA siRNAs (0, 1, 5, 10, 20 and 100nM) resulted in reduced cell cycle of hiPSC-CMs in a dose-dependent reduction in the cell cycle of hiPSC-CMs (Supplemental Figure 8A-8C). Additionally, a low dose (1nM) of miR-197-3p mimics promoted cell cycle, whereas high doses of miR-197-3p and miR215-3p mimics (100nM) reduced cell cycle. Furthermore, inhibiting miR-140-5p with a high dose of miRNA siRNAs or miR-15a-3p with various concentrations of miRNA siRNAs resulted in a reduced cell cycle of hiPSC-CMs. Similarly, a high dose of miR-140-5p siRNAs and various

concentrations of miR-140-5p mimics also led to a reduction of the cell cycle (Supplemental Figure 8D). Moreover, when low doses (1 and 5nM) of miRNA siRNAs were used to inhibit miR-128-3p, it promoted the cell cycle of hiPSC-CMs (Supplemental Figure 8F). However, high doses of miRNA siRNAs and activation with different concentrations of mimics both led to a decreased cell cycle of hiPSC-CMs.

Expression of miR-128 increases in postnatal mouse hearts. Overexpression of miR-128 inhibits and knockout of miR-128 promotes the cell cycle of neonatal mouse cardiomyocytes (47). The function of miR-128 in pig or human cardiomyocytes remains unknown. Therefore, we determined the impact of inhibition or activation of miR-128-3p on the expression of “upstream” circRNA and “downstream” mRNAs using qRT-PCR, and on the cell cycle of hiPSC-CMs via bioluminescent assay and immunostaining using antibodies against BrdU and PH3. qRT-PCR confirmed the increased expression of miR-128-3p in hiPSC-CMs treated with 5nM of has-miR-128-3p mimics, which resulted in reduced expression of has-AC096949_0001 (Supplemental Figure 9A-9B). Additionally, has-miR-128-3p mimics decreased the cell cycle of hiPSC-CMs as indicated by the reduced bioluminescent signal compared to control, along with a decrease in the prevalence of BrdU- and PH3-positive cells (Supplemental Figure 9C-9E). This data is consistent with our previous finding that siRNA-mediated inhibition of has-AC096949_0001 resulted in a decreased cell cycle of hiPSC-CMs (Figure 5I-5J, 6A-6B, and 7A-7B). Furthermore, has-miR-128-3p mimics reduced the expression of membrane metalloendopeptidase (MME) (Supplemental Figure 9F). On the other hand, inhibiting the expression of miR-128-3p in hiPSC-CMs treated with 5nM of has-miR-128-3p siRNAs

resulted in increased expression of has-AC096949_0001 (Supplemental Figure 10A-10B). Additionally, has-miR-128-3p siRNAs increased the cell cycle of hiPSC-CMs as shown by the increased bioluminescent signal compared to control, as well as an enhanced prevalence of BrdU- and PH3-positive cells which suggested an increased cell cycle (Supplemental Figure 10C-10E). Furthermore, has-miR-128-3p mimics increased the expression of MME (Supplemental Figure 10F). In the future, more research is needed to study the cell cycle function of MME and to validate other miRNAs and mRNAs in the circRNA-miRNA-mRNA network to identify new pathways for regulating cardiomyocyte proliferation and regeneration. Overall, these results suggest the potential effects of RNA interactions on the regulation of cardiomyocyte cell cycle.

Discussion

In recent years, there has been an increasing amount of evidence indicating the imporant role of circRNAs in various physiological and pathological processes related to human health and disease (48-50). However, the expression and function of circRNAs in the hearts of large mammals are largely unknown. In the current study, we examined the expression patterns of circRNAs in pig hearts at different postnatal stages (P1, P3, P7, and P28) (Figure 1). circRNAs that were found to be differentially expressed in this study were mainly linked to host genes that are involved in a variety of processes including cell division, apoptosis, angiogenesis, immune responses, muscle development, transition between epithelial and mesenchymal cells, and metabolism (Figure 1E-1H). Some of

these pathways are closely linked to cardiomyocyte cell cycle and proliferation, which is pivotal for myocardial regeneration.

Cardiomyocyte cell cycle and heart regeneration are intricate processes that involve the coordinated expression of numerous genes and regulatory molecules. Recently, circRNAs have emerged as important contributors in these processes, functioning as essential regulators of gene expression through various mechanisms. Huang et al. investigated the roles of circNfix in adult mice post myocardial infarction (10). Their data suggested that inhibition of circNfix promoted cardiomyocyte proliferation and improved heart function. Si et al. discovered that circHipk3 overexpression promotes cardiomyocyte proliferation by increasing Notch1 intracellular domain (N1ICD) acetylation, thereby increasing the N1ICD stability and preventing its degradation. Furthermore, adeno-associated virus 9 (AAV9)-mediated overexpression of circHipk3 induces cardiac regeneration and improves heart function in adult mice post myocardial infarction (11). Zhang et al. reported that circCDYL overexpression promotes proliferation of cardiomyocytes in vitro, and AAV9-mediated overexpression of circCDYL improves heart function in adult mice post myocardial infarction (12). Ma et al. reported that inhibiting the expression of circMdc1 increases cardiomyocyte cell cycle activity. In addition, the cardiac-specific AAV-mediated knockdown of circMdc1 promotes cardiac regeneration in both neonatal and adult mice after myocardial infarction (13). These studies collectively highlight the important role of circRNAs in regulating the cell cycle of cardiomyocytes and the process of heart regeneration. By affecting gene expression through interactions with

miRNAs and other regulatory molecules, circRNAs present as potential targets for therapeutic interventions aimed at improving cardiac repair and regeneration.

Our study identified 10 new circRNAs associated with the cell cycle in pig hearts, and whose expression patterns changed dynamically during cardiomyocyte maturation (Figure 4). To investigate these 10 circRNAs' roles in cardiomyocyte cell cycle regulation, we matched them with their human counterparts (Supplemental table 5) and conducted phenotypic validation on hiPSC-CMs in culture. Six circRNAs potentially involved in cell cycle regulation were identified. Knocking down some of these circRNAs changed cell cycle activity in hiPSC-CMs (Figure 5-7). These results highlight the complex regulatory roles of circRNAs in heart development and their potential implications in myocardial regeneration. In terms of potential therapeutic strategies for cardiovascular diseases, inhibition of hsa-ABLIM1_0001, hsa-RNF13_0004 and hsa-KIF1B_0001, or overexpression of hsa-MYOM1_0001, hsa-AC096949_0001, and hsa-PDLIM5_0001 may be promising in promoting cardiomyocyte cell cycle and heart regeneration. These findings demonstrate significant changes in circRNA expression in neonatal pig hearts with remarkable regenerative abilities, highlighting the vital role of circRNAs during early postnatal heart development of pig hearts. Further investigations are needed to uncover the specific functions and mechanisms of these circRNAs in regulating cardiomyocyte cell cycle in vivo.

Mechanisms underlying the function of circRNAs in cardiomyocyte cell cycle remain unclear. It has been reported that endogenous RNAs (ceRNAs) may function by

sequestering miRNAs and modulating target mRNA expression (4). In order to obtain a deeper understanding of the regulatory function of circRNAs in cell proliferation, we conducted miRNA sequencing (Figure 2) and mRNA sequencing (Figure 3) for neonatal pig hearts and constructed a comprehensive circRNA-miRNA-mRNA network using Cytoscape (46). This approach allows us to uncover the potential regulatory pathways that target the cell cycle pathways of cardiomyocytes. We predicted 11 corresponding miRNAs and 45 target mRNAs that are associated with the cell cycle function of the five circRNAs (Supplemental Figure 7A-7C). Specifically, interactions between circRNAs, miRNAs, and mRNAs were predicted and used to construct a circRNA-miRNA-mRNA regulatory network. Five conserved pig circRNAs (CDH13_0001, sus-ABLIM1_0001, sus-RNF13_0002, sus-KIF1B_0001, and sus-AGL_0001) and their corresponding miRNAs were analyzed using circAtlas(v2) and miRNAtap package. Cytoscape software was utilized to construct their corresponding circRNA-miRNA-mRNA regulatory network, providing insight into potential cell proliferation mechanisms. These findings suggest that these circRNAs may regulate the cell cycle through specific miRNA interactions. However, it is crucial to validate these predictions through phenotype experiments.

circRNA sequencing has been performed in heart samples from mice, rats, pigs, and humans as well as the cardiomyocytes derived from hiPSCs or hiESCs (51-58). Liang et al. conducted total RNA sequencing in different organs (including the heart, liver, spleen, lung, kidney, ovarium, testis, skeletal muscle, and fat) of 3 adult pigs (240 days after birth), and identified 205 unique circRNAs in the heart (57). Mester-Tonczar et al. performed RNA sequencing of rRNA-depleted RNA samples from infarcted and healthy myocardium

tissue samples of six female adult pigs (6 months old) and discovered that the expression of Circ-RCAN2 and circ-C12orf29 were significantly downregulated in infarcted tissue compared to healthy pig heart (59). However, majority of the RNA Sequencing was done on heart samples from animals or human hearts with heart failure. Thus far, there has been no RNA sequencing performed in postnatal hearts at different ages. There are several advantages in our study. First, to increase the coverage and the quality of our circRNA sequencing data, we sent samples to two different companies (i.e., Novogene Inc, and CD genomics Inc). Prior to downstream analysis, batch correction of these two datasets was done as described in DESeq2 Bioconductor package. Second, we conducted qRT-PCR experiments to validate RNA sequencing data, and the results concurred with the circRNA-seq data (Figure 4). Existing approaches for circRNA identification primarily rely on detecting reads spanning backsplice junctions (BSJs), without differentiating between linear and circular reads that align to the internal regions of circRNAs (60). In contrast, our method involves transcribed cDNA molecules containing multiple copies of the corresponding full-length circRNA sequence, and each long read provides direct evidence of a circRNA's presence and sequence (61). Additionally, we employed qRT-PCR to validate the reliability of circRNA quantification, randomly selecting circRNAs to enhance the applicability of this approach to circRNA studies (62). To improve the accuracy of circRNA identification, we excluded candidates lacking canonical AG/GT splice sites and candidates mapped to the mitochondrial genome (63).

There are limitations in our study. First, although we have included six samples in each group, it would be beneficial to further increase the sample size. Second, because of the lack of a pig cardiomyocyte cell line and limited availability of pig databases for analyzing mRNA and miRNAs, we chose to use conserved human circRNAs to construct the circRNA-miRNA-mRNA network. Third, the RNA sequencing was performed using samples from the entire heart, which contain both myocytes and non-myocytes.

In summary, data from the current study improved our understanding of the essential roles played by circRNAs in the development of pig hearts, and uncovered new insights into potential mechanisms that drive cell proliferation through the exploration of circRNAs. To our knowledge, this is the first report about circRNA profiles in the postnatal hearts of large mammals. Although we acknowledge limitations such as sample variation and the need for further validation, our findings will greatly enhance our understanding of circRNA function and its potential implications in heart development and maturation in large mammals. It was reported that modulating the expression of circRNAs confers cardioprotection in preclinical animal models of heart failure (19, 64, 65). In this study, we identified and validated six circRNAs that regulate cardiomyocyte cell cycle and proliferation. We also matched these pig circRNAs to human circRNAs and constructed the circRNA-miRNA-mRNA network. As a next step, we will validate the potential roles of these circRNAs in regulating myocardial regeneration in pig hearts and explore potential small molecules that may regulate the expression of the circRNAs. Therefore, the successful identification of the circRNAs that control heart regeneration in pigs will provide new therapeutic targets for the treatment of heart failure in humans.

Methods

Experimental animals and sex as a biological variable. The hearts of domestic Yorkshire pigs (Premier Biosource, Inc) at postnatal day 1 (P1), 3 (P3), 7 (P7), and 28 (P28) were isolated. These hearts were rinsed in cold saline immediately, and frozen in liquid nitrogen. A total of six animal hearts including both male and females were used from each age group, and similar findings are reported for both sexes. RNA sequencing of mRNAs and noncoding RNAs including circRNAs and miRNAs was performed using these samples. qRT-PCR was then used for data validation. Information on key reagents were listed in Supplemental table 6, and primary and secondary antibodies in Supplemental table 7.

Total RNA extraction and qRT-PCR. The RNeasy Mini Kit (Qiagen) was used to extract total RNA from pig heart tissue and hiPSC-CMs. The concentration of RNA in the samples was determined by measuring the absorbance at 260 nm using UV spectrophotometry, specifically with the Nanodrop 2000 instrument (Thermo Fisher Scientific, Inc). The High-Capacity cDNA Reverse Transcription Kit (Applied Biosystems, Inc) was used to generate complementary DNA (cDNA). qRT-PCR was performed using the SYBR Green PCR Master Mix (Roche, Inc). The primer sequences used in this experiment were listed in Supplemental table 8. Each qRT-PCR reaction was conducted in triplicate using an LightCycler® 480 System instrument (Roche, Inc). To ensure accurate normalization,

gene expression values were normalized to the average expression of the housekeeping gene GAPDH.

circRNA sequencing. The quality of the RNA samples was evaluated using High Sensitivity RNA Tapestation system (Agilent Technologies Inc). Quantification of RNA was performed using Qubit 2.0 RNA High Sensitivity (HS) assay (Thermo Fisher Inc). Depletion of ribosomal RNA (rRNA) was performed using RiboZero Gold kit based on the instructions. Next, RNaseR buffer and RNaseR were added to the rRNA-depleted samples to remove linear RNA. Construction of the library was performed according to the instructions provided by the manufacturer for the NEBNext Ultra II RNA (Directional) kit. The quantity of the final library was measured using KAPA SYBR FAST qPCR, and the quality of the library was assessed using the TapeStation D1000 ScreenTape (Agilent Technologies Inc). Illumina 8-nt dual-indices were used for library indexing. Equimolar pooling of the libraries was performed based on quality control values. The libraries were subsequently sequenced on an Illumina sequencer (Illumina Inc., CA) with a read length configuration of 150 paired-end reads. The goal was to obtain 20 million paired-end reads per sample (20M in each direction).

Small RNA sequencing. RNA sample quality was assessed using the High Sensitivity RNA Tapestation and quantified with the Qubit 2.0 RNA HS assay. Construction of the library was performed according to the instructions provided by the manufacturer for the NEBNext Small RNA Library Prep kit. In brief, the 3' SR adapter was ligated to the RNA. Subsequently, reverse transcriptase with SR RT Primer were used to generate first strand

cDNA, followed by the ligation of the 5´ SR Adaptor and synthesis of the second strand cDNA. The resulting products were purified and enriched through PCR to create the final cDNA library. Fragments within the range of 140-160 bp (including miRNAs with lengths of 18-40 bp and adapters/barcodes with length of 120 bp) were selected. The quantity of the final library was measured using KAPA SYBR FAST qPCR, and the library quality was assessed using the TapeStation D1000 ScreenTape. Equimolar pooling of libraries was performed based on quality control values, and sequencing was carried out on an Illumina sequencer with a read length configuration of 150 paired-end, generating 10 million paired-end reads per sample (20 million in each direction).

Total RNA sequencing. The quality of the RNA samples was evaluated using the High Sensitivity RNA Tapestation system. Quantification of RNA was measured utilizing the Qubit 2.0 RNA High Sensitivity assay. Ribosomal RNA (rRNA) was removed using the RiboZero Gold kit based on the manufacturer's instructions. Library construction was performed following the manufacturer's instruction for the TruSeq Stranded Total RNA kit. This process requires breaking down the RNA into smaller pieces by using divalent cations at higher temperatures (typically around 70-95°C). Cleaved RNA fragments were then reverse transcribed into first strand cDNA using reverse transcriptase and random primers, followed by the synthesis of second strand cDNA. Resulting cDNA fragments were modified with a single 'A' base and ligated with an adapter. The resulting products underwent purification and PCR enrichment to generate the final cDNA library. The size of library inserts typically ranges from 120–200 bp, with a median size of 150 bp. The final library quantity was determined using KAPA SYBR FAST qPCR, and the library quality

was evaluated using the TapeStation D1000 ScreenTape. Equimolar pooling of libraries was performed based on quality control values. Pooled libraries were sequenced on an Illumina sequencer with a read length configuration of 150 paired-end reads. The goal was to obtain 100 million paired-end reads per sample (20 million in each direction). Since RNA was fragmented at the beginning without size selection, it was anticipated that the subsequent library would contain both coding and non-coding RNA fragments, including long non-coding RNAs (lncRNAs). Utilization of rRNA-depleted RNAs as input enhanced the chances of maintaining non-coding RNAs in the final library. As a result, the sequencing data exhibited the presence of non-coding RNAs, enabling the analysis of both coding and non-coding transcripts, including lncRNAs.

Identification and quantification of circRNAs. Cross sample quality control check using metrics like percentage of uniquely mapped reads and GC content, along with their visualization was done using MultiQC (v1.11) (66). Index generation and paired-end alignment of each sample were performed using STAR (v2.7.9a), with the *chimSegmentationMin* parameter set to 10 (67). Ensemble's reference genome Sscrofa10.2 was used for alignment. This process resulted in the generation of chimeric junctions for each sample. CIRCexploler2 (v2.3.5) was utilized to generate back-splice junctions through its *parse* command (68). The resulting *.bed* files from CIRCexploler2's *parse* step were then used to annotate circRNAs, resulting in an output of known annotated circRNAs. To enable generation of a cross-sample comparable circRNA count matrix for downstream analysis, normalization of the number of back-spliced reads per million mapped reads of circRNA was performed. This led to the generation of two

different circRNA count data (one from CD Genomics data and one from Novogene data). Majority (~97%) of our quantified circRNAs overlapped with circRNAs that have been reported before and were labeled as per the pig annotation in circAtlas(v2). The rest of the unlabeled circRNAs were given novel names. Specifically, novel circRNAs were named with first prefix annotating the species, followed by host gene name, and lastly the unique ID annotated by our lab followed by a unique index. For example, *sus-AGL_VLJW2* was a novel circRNA identified in our study, with first prefix indicating that it is from the pig species, located in *AGL* host gene and the last prefix VLJW2 interpreting it as the second novel circRNA found in this specific host gene (*AGL*). In addition, we obtained quantified mRNA data with ~6640 protein coding genes, and quantified miRNA expression data with ~338 miRNAs described in experimental design section above, for our integrated downstream analysis steps below.

Differential expression analysis and pathway enrichment analysis. circRNA expression data with a total of 24 pig samples from CD Genomics and Novogene was combined using bedtool's *intersection* command (69). First, batch correction of the pig samples from Novogene and CD Genomics was carried out using DESeq2 package in R (70). The batch-corrected samples were then visualized using DESeq2's multidimensional scaling (MDS) plot and Linnorm's hierarchical clustering of samples plot (71). Based on the MDS plot, one sample from Novogene on day 28 failed to correct for the batch effect and was excluded. Lowly expressed circRNAs were filtered, retaining only circRNAs with at least 10% of the samples with counts $\geqslant$ 3. This resulted in ~7000 filtered and batch corrected circRNAs. To investigate differences in circRNA expression across neonatal pig's

developmental stages, we conducted differential expression analysis of circRNA host genes under different experimental designs: day 1 vs day 3 (P1 vs P3), day 1 vs day 7 (P1 vs P7), day 1 vs day 28 (P1 vs P28), and day 1 vs days 3, 7, and 28 (P1 vs P3, P7, and P28). This differential analysis was performed using R packages DESeq2 and Linnorm. Volcano plots were generated using ggplot2 package in R for each defined experimental design above (72). circRNAs with a log two-fold change were considered upregulated if $log_2FC > 0.5$, or downregulated if $log_2FC < -0.5$. If a circRNA was upregulated or downregulated and had an p-value $\leqslant 0.05$, it was considered as significant. Since both mRNA and miRNA data were sequenced in one batch and from one company (CD Genomics, Inc), batch correction step was skipped. Lastly, differential expression analysis was repeated for our miRNA data and mRNA data, using the same experimental designs as described for circRNA above. Results from differential expression analysis of our circRNA and mRNA data were used for pathway enrichment analysis. Specifically, to investigate enriched pathways during different stages of heart development and to identify the corresponding transcripts associated with these enrichments, pathway enrichment analysis of circRNA host genes and of mRNAs was conducted using the R packages ReactomePA and ClusterProfiler (73, 74).

Prediction of circRNA to the targeted miRNAs and miRNAs. Majority (~97%) of our quantified circRNAs were annotated as per circAtlas(v2). This database not only provides the circRNA of interest but also includes all other reported conserved circRNAs from six different species, including pig, mouse, and human. Additionally, the database provides information about the tissue in which the circRNA of interest is expressed. Because

resources for predicting/annotation of pig circRNA to their miRNA target(s) are currently unavailable, for our selected circRNA of interests, we utilized corresponding conserved human circRNA as annotated in circAtlas(v2). As such, for the pig circRNAs conserved in human, circAtlas(v2) was used to link them to their corresponding miRNAs detected in miRanda (75) and TargetScan (76).

Using the predicted miRNA targets above, corresponding target gene(s) were predicted using miRNAtap (v1.6.0) package in R (45). Specifically, the function *getPredictedTargets(min_src=2)* in miRNAtap was used to predict target genes using 5 different aggregation databases: miRanda (103), TargetScan (104), DIANA (77), PicTar (78), and miRDB (79), with the parameter *min_src=2* ensuring high confidence prediction of targets reported in at least 2 of these databases. The top 54 highly scored mRNA targets were selected. Finally, of these predicted miRNAs to mRNA target genes, a filtering was done to retain those expressed in our mRNA data.

Culture and differentiation of human induced pluripotent stem cells. The hiPSC line was purchased from WiCells Inc (Cat: FTDL-01, WI), and genetically modified to express a luciferin reporter gene under a cardiac-specific troponin T promoter as we described previously (80). These hiPSCs were cultured on Matrigel Membrane Matrix (Thermo Fisher Scientific, Cat: CB356253) using mTeSR™ Plus basal medium supplemented with appropriate supplements until 80%-100% confluency. Subsequently, the hiPSCs were differentiated into cardiomyocytes using the protocol we described before (80). In brief, the cells were cultured in basal medium for 24 hours, which consisted of RPMI 1640

medium supplemented with 2% B27 supplement minus insulin, along with CHIR99021 (a GSK-3 inhibitor). Then, 2 mL and 1 mL more basal medium were added separately in the next two days. After 72 hours of culture, IWR-1 (a Wnt inhibitor) was added, and the cells were cultured for an additional 48 hours. The medium was then changed every two days. On day 9, the medium was replaced with RPMI 1640 medium containing 2% B27 supplement. hiPSC-CMs typically began to beat at 9-12 days after the initiation of differentiation. The hiPSC-CMs were purified using metabolic selection as we described before (80). In brief, the medium was replaced with glucose-free RPMI 1640 medium supplemented with 2% B27, and the medium was changed every three days until four weeks after the initiation of cardiac differentiation. This method produced hiPSC-CMs with a purity exceeding 90% as we reported before (80).

siRNA-based knocking down of circRNAs. Four weeks after differentiation, hiPSC-CMs were plated either in 96-well plates (for bioluminescent analysis, 50,000 cells per well) or 2-well chamber slides (for histology studies, 50,0000 cells per well), respectively. The cells were incubated in medium (RPMI 1640 medium containing 2% B27 supplement) at 37^0C for 48 hours. The transfection mixture was prepared by supplementing the fresh culture medium with the transfection reagents (Lipofectamine™ RNAiMAX) and either negative control siRNA or siRNAs targeting specific circRNAs. The concentrations of siRNAs used were 10, 40, or 80 nM (as shown in Supplemental table 9). On the day of siRNA transfection, the cells were washed once with phosphate-buffered saline, and then incubated with transfection mixture. Both the transfection reagent and siRNA at different concentrations were diluted 1:1 in serum-free Opti-MEM and incubated for 5 minutes at

room temperature before being used to treat the cells. Functional experiments (bioluminescent analysis and histology studies) were conducted three days after siRNA treatments. Efficiency of siRNA-based circRNA knockdown was evaluated using qRT-PCR using primers listed in Supplemental table 8. The siRNA experiments in Figures 6 and 7 shared the same controls.

Evaluation of cardiomyocyte cell cycle via bioluminescence assay and immunohistology. After the miRNA siRNA or mimic transfection, bioluminescence assays were performed by adding the D-Luciferin reagents and measuring bioluminescence signal intensity using the IVIS-100 In Vivo Imaging System (PerkinElmer, Inc) as we described before (41, 42, 80). The radiance signals obtained from the bioluminescence assay were recorded for each group of cells. Next, a standard curve was generated by plotting a linear regression curve of cell numbers vs. the respective radiance obtained from the bioluminescence assay for each cell densities. The standard curve allowed us to determine the cell number from the bioluminescence signal obtained from each well of the 96-well plate.

For immunohistology, the cells were fixed in 4% paraformaldehyde for 15 minutes, followed by permeabilization with 0.25% Triton X-100 for another 15 minutes at room temperature. The samples were incubated with blocking solution (10% donkey serum in DPBS, pH 7.4) for one hour at room temperature. Subsequently, the samples were incubated with primary antibodies (as shown in Supplemental table 7), including anti-BrdU and anti-phosphorylated histone H3 (PH3) antibodies, at 1:100 dilutions in blocking buffer overnight at 4°C. For the secondary antibody incubation, a 1:100 dilution in blocking

buffer was used, and the samples were incubated for 1 hour at room temperature. Nuclei were counterstained with 4,6-diamidino-2-phenyl-indole (DAPI). Images from 30 randomly selected high-power fields were taken to evaluate cell proliferation. Cells in the S-phase of the cell cycle were identified by analyzing BrdU incorporation and quantified as a percentage of positively stained cardiomyocytes. Likewise, cells in the M-phase of the cell cycle were identified by analyzing the expression of PH3 and quantified as the percentage of positively stained cardiomyocytes.

miRNA overexpression and siRNA-based knocking down. The hiPSC-CMs were seeded either in 6-well plates (for qPCR analysis, with 2000,000 cells per well) or 2-well chamber slides (for histology studies, 50,0000 cells per well). The cells were then incubated in medium (RPMI1640 medium containing 2% B27 supplement) at 37^0C for 48 hours. The transfection mixture was prepared by adding transfection reagents (Lipofectamine™ RNAiMAX) to the fresh culture medium along with either miRNA mimics or siRNAs targeting specific miRNAs (see sequences in Supplemental table 10). Different concentrations of mimics or siRNAs (1, 5, 10, 20, 100 nM) were used. Cells that were not treated with miRNA mimic or were treated with negative control siRNAs were used as the control group, respectively. On the day of siRNA transfection, the cells were washed with phosphate-buffered saline (PBS) and then treated with the transfection mixture. Both the transfection reagent and siRNAs at varying concentrations were diluted 1:1 in serum-free Opti-MEM and incubated for 5 minutes at room temperature before being added to the cells. Functional experiments (qPCR analysis and histological studies) were carried out three days after the siRNA treatments. The effectiveness of miRNA overexpression and

siRNA-based miRNA knockdown were assessed by qRT-PCR using primers listed in Supplemental table 11.

Evaluation of circRNA intracellular localization by Immunostaining. The hiPSC-CMs were plated in 2-well chamber slides (~500,000 cells per well for RNA probe studies). The cells were then incubated in RPMI1640 medium containing 2% B27 supplement at 37^0C for 48 hours. The samples were fixed with 4% formaldehyde solution at room temperature for 30 minutes, followed by three times of wash with 2 mL of 1x PBS. Samples were then treated with a detergent solution QC for 5 minutes at room temperature, followed by two washes with 1x PBS. Next, a working protease solution was prepared and added to the slides, followed by a 10-minute incubation. The working probe set solution was prepared using circular RNA probes targeting specific circRNAs designed by Thermo Fisher Scientific Inc. Samples were rinsed with 1x PBS, and then the working probe set solution was applied to the samples with 80 µL of working probe set solution for each sample. This solution contains 0.8 µL of probe set and 79.2 µL of probe set diluent buffer. Samples were incubated for 3 hours at 40°C.The slides were washed with a wash buffer three times and then treated with preamplifier mix, amplifier mix, and label probe mix solutions in separate steps, each followed by incubation and washing with the wash buffer. Subsequently, samples were treated with a working DAPI solution, incubated, and washed with 1x PBS. Finally, samples were prepared for microscopy by adding Prolong® Gold Antifade Reagent and cover glass, before being imaged on an Olympus IX83 microscope at 40x magnification with DAPI, GFP, and AF594 channels.

Time-varying effect modeling (TVEM) of cell cycle regulating circRNAs. To get an overall overview of how our circRNA expression profile changed across time, we performed TVEM analysis of circRNA expression focusing on circRNA host genes that were enriched in cell cycle related pathways. Variables used in the model were defined below. Consider a cell cycle related pathways C_1^i. If G_{all} is the list of all our host genes in our data, then we identify a set of host genes $g_1, g_2 \ldots g_n \in G_c^i$ enriched in cell cycle pathway *i* where $G_c^i \subset G_{all}$. To identify if a specific cell cycle pathways is time dependent, we use our selected gene sets G_c^i as our positive label. We then randomly selected n negative gene sets $G_{noncellCycle}$, such that $G_{noncellCycle} \subset (G_{all} - G_c^i)$. As such for every C_1^i *with n* genes, we have n × 2 response variable Y indicating whether a host gene is in C_1^i or not. Additionally, for each of these selected 2n host genes, we define our explanatory variable *x* as corresponding circRNA expression data. A time variable is also defined based on the postnatal day from which the data came (i.e., time = 1 if sample was from P1, 3 if sample was from P3, and so forth). For each evaluated pathway, we leverage *tvem* package v(1.4.1) (81) in R along with the above defined *2n* × *3* matrix to run the TVEM model as per the equation below

$$y_t \sim \beta_0(t) + \beta_1(t)x(t)$$

We then evaluated the $\beta_1(t)x(t)$ coefficients for different cell cycle related pathways (Supplemental Figure 3).

Statistics. Quantile normalization and subsequent data processing were conducted in R software. The statistical analysis was performed using GraphPad Prism 9 software. All data are presented as the mean ± SEM (standard error of the mean). Statistical

comparisons between two groups were carried out using Student's t-test, with statistical significance defined as $p < 0.05$. For comparisons among multiple groups, one-way ANOVA with Tukey's Honestly Significant Difference test was used, and statistical significance was set at $p < 0.05$.

Study approval. All animal protocols were approved by the Institutional Animal Care and Use Committee (IACUC) of the Mayo Clinic. All animal surgical procedures and euthanasia were performed based on approved IACUC protocol and in accordance with the National Institutes of Health Guide for the Care and Use of Laboratory Animals.

Data availability. All data associated with this study are present in the paper or the supplemental information, and raw data are included in the Supporting Data Values file. Reagents and materials associated with this study are available from the corresponding authors (JW and WZ). RNA Sequencing data has been deposited to a public dataset repository (NCBI GEO; access ID: GSE269522).

Author contributions

LT initiated the project, conducted experiments, acquired and analyzed data, and wrote the manuscript. VN analyzed data and wrote the manuscript. Co–first authorship of LT and VN is reflected by their joint intellectual contributions and writing of this manuscript. Order of co-first authorship was determined by relative experimental and data contributions. PL conducted experiments. JW designed research studies and wrote the manuscript. WZ designed research studies, wrote the manuscript, and handled finance.

Acknowledgements

We are grateful to our laboratory colleagues Alex Patino, Fan Li, Huiliang Qiu, Yura Son, and Evelyn Wang for their invaluable technical support throughout this study.

This work is supported by NIH NHLBI grants (R01 HL142627, HL156855, and HL162747 to W.Z.), NIH NLM grant (R01LM013438 to J.W.), AHA TPA Award (20TPA35490001 to W.Z.), AHA Postdoctoral Fellowship Award (23POST1020047 to L.T.), Mayo Clinic Mandelbaum Family Career Development Award in Cardiovascular Sciences (to L.T.), and Mayo Clinic Center for Individualized Medicine grant (to J.W.).

Address correspondence to: Wuqiang Zhu, Department of Cardiovascular Medicine, Mayo Clinic Arizona, 13400 Shea Blvd, Collaborative Research Building, Room 2-113, Scottsdale, AZ 85259, USA. Phone: 480-301-9693. E-Mail: zhu.wuqiang@mayo.edu. Junwen Wang, Division of Applied Oral Sciences & Community Dental Care, Faculty of Dentistry, The University of Hong Kong, 2A-07, 2/F, Prince Philip Dental Hospital, 34 Hospital Road, Sai Ying Pun, Hong Kong. Phone: 852-2852-0128. E-Mail: junwen@hku.hk

Footnotes

Conflict of interest: The authors have declared that no conflict of interest exists.

REFERENCES

1. Porrello ER, Mahmoud AI, Simpson E, Hill JA, Richardson JA, Olson EN, et al. Transient regenerative potential of the neonatal mouse heart. *Science.* 2011;331(6020):1078-80.
2. Son Y, and Zhu W. Gene Therapy for Cardiomyocyte Renewal: Cell Cycle, a Potential Therapeutic Target. *Mol Diagn Ther.* 2023;27(2):129-40.
3. Zhu W, Zhang E, Zhao M, Chong Z, Fan C, Tang Y, et al. Regenerative Potential of Neonatal Porcine Hearts. *Circulation.* 2018;138(24):2809-16.
4. Tang L, Li P, Jang M, and Zhu W. Circular RNAs and Cardiovascular Regeneration. *Front Cardiovasc Med.* 2021;8:672600.
5. Leng Y, Wang MZ, Xie KL, and Cai Y. Identification of Potentially Functional Circular RNA/Long Noncoding RNA-MicroRNA-mRNA Regulatory Networks Associated with Vascular Injury in Type 2 Diabetes Mellitus by Integrated Microarray Analysis. *J Diabetes Res.* 2023;2023:3720602.
6. Chen QW, Wang DQ, Ding BX, Tang MM, Li XG, Zhou JY, et al. [hsa_circ_0000231 affects the progression of tongue squamous cell carcinoma by activating Wnt/beta-catenin signaling pathway]. *Zhonghua Er Bi Yan Hou Tou Jing Wai Ke Za Zhi.* 2022;57(10):1230-9.
7. Cao Y, Shi Y, Yang Y, Wu Z, Peng N, Xiao J, et al. Urinary exosomes derived circRNAs as biomarkers for chronic renal fibrosis. *Ann Med.* 2022;54(1):1966-76.
8. Huang A, Zheng H, Wu Z, Chen M, and Huang Y. Circular RNA-protein interactions: functions, mechanisms, and identification. *Theranostics.* 2020;10(8):3503-17.
9. Kishore R, Garikipati VNS, and Gonzalez C. Role of Circular RNAs in Cardiovascular Disease. *J Cardiovasc Pharmacol.* 2020;76(2):128-37.
10. Huang S, Li X, Zheng H, Si X, Li B, Wei G, et al. Loss of Super-Enhancer-Regulated circRNA Nfix Induces Cardiac Regeneration After Myocardial Infarction in Adult Mice. *Circulation.* 2019;139(25):2857-76.
11. Si X, Zheng H, Wei G, Li M, Li W, Wang H, et al. circRNA Hipk3 Induces Cardiac Regeneration after Myocardial Infarction in Mice by Binding to Notch1 and miR-133a. *Mol Ther Nucleic Acids.* 2020;21:636-55.
12. Zhang M, Wang Z, Cheng Q, Wang Z, Lv X, Wang Z, et al. Circular RNA (circRNA) CDYL Induces Myocardial Regeneration by ceRNA After Myocardial Infarction. *Med Sci Monit.* 2020;26:e923188.
13. Ma W, Wang X, Sun H, Xu B, Song R, Tian Y, et al. Oxidant stress-sensitive circRNA Mdc1 controls cardiomyocyte chromosome stability and cell cycle re-entry during heart regeneration. *Pharmacol Res.* 2022;184:106422.
14. Bian Y, Pang P, Li X, Yu S, Wang X, Liu K, et al. CircHelz activates NLRP3 inflammasome to promote myocardial injury by sponging miR-133a-3p in mouse ischemic heart. *J Mol Cell Cardiol.* 2021;158:128-39.
15. Huang C, Qu Y, Feng F, Zhang H, Shu L, Zhu X, et al. Cardioprotective Effect of circ_SMG6 Knockdown against Myocardial Ischemia/Reperfusion Injury Correlates with miR-138-5p-Mediated EGR1/TLR4/TRIF Inactivation. *Oxid Med Cell Longev.* 2022;2022:1927260.
16. Xu C, Jia Z, Cao X, Wang S, Wang J, and An L. Hsa_circ_0007059 promotes apoptosis and inflammation in cardiomyocytes during ischemia by targeting microRNA-378 and microRNA-383. *Cell Cycle.* 2022;21(10):1003-19.
17. Geng HH, Li R, Su YM, Xiao J, Pan M, Cai XX, et al. The Circular RNA Cdr1as Promotes Myocardial Infarction by Mediating the Regulation of miR-7a on Its Target Genes Expression. *PLoS One.* 2016;11(3):e0151753.

18. Cai L, Qi B, Wu X, Peng S, Zhou G, Wei Y, et al. Circular RNA Ttc3 regulates cardiac function after myocardial infarction by sponging miR-15b. *J Mol Cell Cardiol.* 2019;130:10-22.
19. Zheng H, Huang S, Wei G, Sun Y, Li C, Si X, et al. CircRNA Samd4 induces cardiac repair after myocardial infarction by blocking mitochondria-derived ROS output. *Mol Ther.* 2022;30(11):3477-98.
20. Liu X, Wang M, Li Q, Liu W, Song Q, and Jiang H. CircRNA ACAP2 induces myocardial apoptosis after myocardial infarction by sponging miR-29. *Minerva Med.* 2022;113(1):128-34.
21. Zhai C, Qian G, Wu H, Pan H, Xie S, Sun Z, et al. Knockdown of circ_0060745 alleviates acute myocardial infarction by suppressing NF-kappaB activation. *J Cell Mol Med.* 2020;24(21):12401-10.
22. Chen TP, Zhang NJ, Wang HJ, Hu SG, and Geng X. Knockdown of circROBO2 attenuates acute myocardial infarction through regulating the miR-1184/TRADD axis. *Mol Med.* 2021;27(1):21.
23. Cheng N, Wang MY, Wu YB, Cui HM, Wei SX, Liu B, et al. Circular RNA POSTN Promotes Myocardial Infarction-Induced Myocardial Injury and Cardiac Remodeling by Regulating miR-96-5p/BNIP3 Axis. *Front Cell Dev Biol.* 2020;8:618574.
24. Zhao Q, Li W, Pan W, and Wang Z. CircRNA 010567 plays a significant role in myocardial infarction via the regulation of the miRNA-141/DAPK1 axis. *J Thorac Dis.* 2021;13(4):2447-59.
25. Luo C, Ling GX, Lei BF, Feng X, Xie XY, Fang C, et al. Circular RNA PVT1 silencing prevents ischemia-reperfusion injury in rat by targeting microRNA-125b and microRNA-200a. *J Mol Cell Cardiol.* 2021;159:80-90.
26. Zhang J, Tang Y, Zhang J, Wang J, He J, Zhang Z, et al. CircRNA ACAP2 Is Overexpressed in Myocardial Infarction and Promotes the Maturation of miR-532 to Induce the Apoptosis of Cardiomyocyte. *J Cardiovasc Pharmacol.* 2021;78(2):247-52.
27. Wang S, Li L, Deng W, and Jiang M. CircRNA MFACR Is Upregulated in Myocardial Infarction and Downregulates miR-125b to Promote Cardiomyocyte Apoptosis Induced by Hypoxia. *J Cardiovasc Pharmacol.* 2021;78(6):802-8.
28. Wang D, Tian L, Wang Y, Gao X, Tang H, and Ge J. Circ_0001206 regulates miR-665/CRKL axis to alleviate hypoxia/reoxygenation-induced cardiomyocyte injury in myocardial infarction. *ESC Heart Fail.* 2022;9(2):998-1007.
29. Jin L, Zhang Y, Jiang Y, Tan M, and Liu C. Circular RNA Rbms1 inhibited the development of myocardial ischemia reperfusion injury by regulating miR-92a/BCL2L11 signaling pathway. *Bioengineered.* 2022;13(2):3082-92.
30. Shao Y, Li M, Yu Q, Gong M, Wang Y, Yang X, et al. CircRNA CDR1as promotes cardiomyocyte apoptosis through activating hippo signaling pathway in diabetic cardiomyopathy. *Eur J Pharmacol.* 2022;922:174915.
31. Li X, Guo L, Wang J, and Yang X. Pro-fibrotic and apoptotic activities of circARAP1 in myocardial ischemia-reperfusion injury. *Eur J Med Res.* 2023;28(1):84.
32. Liu X, Dou B, Tang W, Yang H, Chen K, Wang Y, et al. Cardioprotective effects of circ_0002612 in myocardial ischemia/reperfusion injury correlate with disruption of miR-30a-5p-dependent Ppargc1a inhibition. *Int Immunopharmacol.* 2023;117:110006.
33. Sun G, Shen JF, Wei XF, and Qi GX. Circular RNA Foxo3 Relieves Myocardial Ischemia/Reperfusion Injury by Suppressing Autophagy via Inhibiting HMGB1 by Repressing KAT7 in Myocardial Infarction. *J Inflamm Res.* 2021;14:6397-407.
34. Zhou LY, Zhai M, Huang Y, Xu S, An T, Wang YH, et al. The circular RNA ACR attenuates myocardial ischemia/reperfusion injury by suppressing autophagy via modulation of the Pink1/FAM65B pathway. *Cell Death Differ.* 2019;26(7):1299-315.

35. Jin P, Li LH, Shi Y, and Hu NB. Salidroside inhibits apoptosis and autophagy of cardiomyocyte by regulation of circular RNA hsa_circ_0000064 in cardiac ischemia-reperfusion injury. *Gene.* 2021;767:145075.
36. Ju J, Li XM, Zhao XM, Li FH, Wang SC, Wang K, et al. Circular RNA FEACR inhibits ferroptosis and alleviates myocardial ischemia/reperfusion injury by interacting with NAMPT. *J Biomed Sci.* 2023;30(1):45.
37. Garikipati VNS, Verma SK, Cheng Z, Liang D, Truongcao MM, Cimini M, et al. Circular RNA CircFndc3b modulates cardiac repair after myocardial infarction via FUS/VEGF-A axis. *Nat Commun.* 2019;10(1):4317.
38. Wang Y, Zhao R, Shen C, Liu W, Yuan J, Li C, et al. Exosomal CircHIPK3 Released from Hypoxia-Induced Cardiomyocytes Regulates Cardiac Angiogenesis after Myocardial Infarction. *Oxid Med Cell Longev.* 2020;2020:8418407.
39. Wu N, Li C, Xu B, Xiang Y, Jia X, Yuan Z, et al. Circular RNA mmu_circ_0005019 inhibits fibrosis of cardiac fibroblasts and reverses electrical remodeling of cardiomyocytes. *BMC Cardiovasc Disord.* 2021;21(1):308.
40. Liberzon A, Birger C, Thorvaldsdottir H, Ghandi M, Mesirov JP, and Tamayo P. The Molecular Signatures Database (MSigDB) hallmark gene set collection. *Cell Syst.* 2015;1(6):417-25.
41. Fan C, Fast VG, Tang Y, Zhao M, Turner JF, Krishnamurthy P, et al. Cardiomyocytes from CCND2-overexpressing human induced-pluripotent stem cells repopulate the myocardial scar in mice: A 6-month study. *J Mol Cell Cardiol.* 2019;137:25-33.
42. Zhu W, Zhao M, Mattapally S, Chen S, and Zhang J. CCND2 Overexpression Enhances the Regenerative Potency of Human Induced Pluripotent Stem Cell-Derived Cardiomyocytes: Remuscularization of Injured Ventricle. *Circ Res.* 2018;122(1):88-96.
43. Zhao M, Fan C, Ernst PJ, Tang Y, Zhu H, Mattapally S, et al. Y-27632 preconditioning enhances transplantation of human-induced pluripotent stem cell-derived cardiomyocytes in myocardial infarction mice. *Cardiovasc Res.* 2019;115(2):343-56.
44. Jie M, Feng T, Huang W, Zhang M, Feng Y, Jiang H, et al. Subcellular Localization of miRNAs and Implications in Cellular Homeostasis. *Genes (Basel).* 2021;12(6).
45. Pajak M, and Simpson TI. miRNAtap: miRNAtap: microRNA Targets - Aggregated Predictions. R package version 1.34.0. https://bioconductor.org/packages/release/bioc/html/miRNAtap.html.
46. Shannon P, Markiel A, Ozier O, Baliga NS, Wang JT, Ramage D, et al. Cytoscape: a software environment for integrated models of biomolecular interaction networks. *Genome Res.* 2003;13(11):2498-504.
47. Huang W, Feng Y, Liang J, Yu H, Wang C, Wang B, et al. Loss of microRNA-128 promotes cardiomyocyte proliferation and heart regeneration. *Nat Commun.* 2018;9(1):700.
48. Wang H, Xiao Y, Wu L, and Ma D. Comprehensive circular RNA profiling reveals the regulatory role of the circRNA-000911/miR-449a pathway in breast carcinogenesis. *Int J Oncol.* 2018;52(3):743-54.
49. Wang M, Su P, Liu Y, Zhang X, Yan J, An X, et al. Abnormal expression of circRNA_089763 in the plasma exosomes of patients with post-operative cognitive dysfunction after coronary artery bypass grafting. *Mol Med Rep.* 2019;20(3):2549-62.
50. Hansen TB, Jensen TI, Clausen BH, Bramsen JB, Finsen B, Damgaard CK, et al. Natural RNA circles function as efficient microRNA sponges. *Nature.* 2013;495(7441):384-8.
51. Werfel S, Nothjunge S, Schwarzmayr T, Strom TM, Meitinger T, and Engelhardt S. Characterization of circular RNAs in human, mouse and rat hearts. *J Mol Cell Cardiol.* 2016;98:103-7.
52. Shen L, Zhang S, Li Q, Fu Y, Tang G, Jiang Y, et al. The Landscape of Non-Coding RNA in an Adult Pig Model of Intrauterine Growth Restriction. *Cell Physiol Biochem.* 2018;50(5):1764-78.

53. Dong K, He X, Su H, Fulton DJR, and Zhou J. Genomic analysis of circular RNAs in heart. *BMC Med Genomics.* 2020;13(1):167.
54. Xia X, Zhang K, Luo G, Cen G, Cao J, Huang K, et al. Downregulation of miR-301a-3p sensitizes pancreatic cancer cells to gemcitabine treatment via PTEN. *Am J Transl Res.* 2017;9(4):1886-95.
55. Lei W, Feng T, Fang X, Yu Y, Yang J, Zhao ZA, et al. Signature of circular RNAs in human induced pluripotent stem cells and derived cardiomyocytes. *Stem Cell Res Ther.* 2018;9(1):56.
56. Tan WL, Lim BT, Anene-Nzelu CG, Ackers-Johnson M, Dashi A, See K, et al. A landscape of circular RNA expression in the human heart. *Cardiovasc Res.* 2017;113(3):298-309.
57. Liang G, Yang Y, Niu G, Tang Z, and Li K. Genome-wide profiling of Sus scrofa circular RNAs across nine organs and three developmental stages. *DNA Res.* 2017;24(5):523-35.
58. Xiao Y, Oumarou DB, Wang S, and Liu Y. Circular RNA Involved in the Protective Effect of Malva sylvestris L. on Myocardial Ischemic/Re-Perfused Injury. *Front Pharmacol.* 2020;11:520486.
59. Mester-Tonczar J, Einzinger P, Winkler J, Kastner N, Spannbauer A, Zlabinger K, et al. Novel Identified Circular Transcript of RCAN2, circ-RCAN2, Shows Deviated Expression Pattern in Pig Reperfused Infarcted Myocardium and Hypoxic Porcine Cardiac Progenitor Cells In Vitro. *Int J Mol Sci.* 2021;22(3).
60. Jia GY, Wang DL, Xue MZ, Liu YW, Pei YC, Yang YQ, et al. CircRNAFisher: a systematic computational approach for de novo circular RNA identification. *Acta Pharmacol Sin.* 2019;40(1):55-63.
61. Chen B, Yi J, Xu Y, Zheng P, Tang R, and Liu B. Construction of a circRNA-miRNA-mRNA network revealed the potential mechanism of Buyang Huanwu Decoction in the treatment of cerebral ischemia. *Biomed Pharmacother.* 2022;145:112445.
62. Panda AC, and Gorospe M. Detection and Analysis of Circular RNAs by RT-PCR. *Bio Protoc.* 2018;8(6).
63. Ye CY, Zhang X, Chu Q, Liu C, Yu Y, Jiang W, et al. Full-length sequence assembly reveals circular RNAs with diverse non-GT/AG splicing signals in rice. *RNA Biol.* 2017;14(8):1055-63.
64. Zhang Y, and Chen B. Silencing circ_0062389 alleviates cardiomyocyte apoptosis in heart failure rats via modulating TGF-beta1/Smad3 signaling pathway. *Gene.* 2021;766:145154.
65. Hu X, Liao W, Teng L, Ma R, and Li H. Circ_0001312 Silencing Suppresses Doxorubicin-Induced Cardiotoxicity via MiR-409-3p/HMGB1 Axis. *Int Heart J.* 2023;64(1):71-80.
66. Ewels P, Magnusson M, Lundin S, and Käller M. MultiQC: summarize analysis results for multiple tools and samples in a single report. *Bioinformatics.* 2016;31(1367-4811 (Electronic)):3047-8.
67. Dobin A, Davis CA, Schlesinger F, Drenkow J, Zaleski C, Jha S, et al. STAR: ultrafast universal RNA-seq aligner. *Bioinformatics.* 2013;29(1):15-21.
68. Zhang XO, Dong R, Zhang Y, Zhang JL, Luo Z, Zhang J, et al. Diverse alternative back-splicing and alternative splicing landscape of circular RNAs. *Genome Res.* 2016;26(9):1277-87.
69. Quinlan AR, and Hall IM. BEDTools: a flexible suite of utilities for comparing genomic features. *Bioinformatics.* 2010;26(6):841-2.
70. Love MI, Huber W, and Anders S. Moderated estimation of fold change and dispersion for RNA-seq data with DESeq2. *Genome Biol.* 2014;15(12):550.
71. Yip SH, Wang P, Kocher JA, Sham PC, and Wang J. Linnorm: improved statistical analysis for single cell RNA-seq expression data. *Nucleic Acids Res.* 2017;45(22):e179.
72. Villanueva RAM, and Chen ZJ. ggplot2: Elegant Graphics for Data Analysis (2nd ed.). *Measurement: Interdisciplinary Research and Perspectives.* 2019;17(3):160-7.
73. Yu G, Wang LG, Han Y, and He QY. clusterProfiler: an R package for comparing biological themes among gene clusters. *OMICS.* 2012;16(5):284-7.
74. Yu G, and He QY. ReactomePA: an R/Bioconductor package for reactome pathway analysis and visualization. *Mol Biosyst.* 2016;12(2):477-9.

75. Enright AJ, John B, Gaul U, Tuschl T, Sander C, and Marks DS. MicroRNA targets in Drosophila. *Genome Biol.* 2003;5(1):R1.
76. Friedman RC, Farh KK, Burge CB, and Bartel DP. Most mammalian mRNAs are conserved targets of microRNAs. *Genome Res.* 2009;19(1):92-105.
77. Maragkakis M, Alexiou P, Papadopoulos GL, Reczko M, Dalamagas T, Giannopoulos G, et al. Accurate microRNA target prediction correlates with protein repression levels. *BMC Bioinformatics.* 2009;10:295.
78. Krek A, Grun D, Poy MN, Wolf R, Rosenberg L, Epstein EJ, et al. Combinatorial microRNA target predictions. *Nat Genet.* 2005;37(5):495-500.
79. Griffiths-Jones S, Saini HK, van Dongen S, and Enright AJ. miRBase: tools for microRNA genomics. *Nucleic Acids Res.* 2008;36(Database issue):D154-8.
80. Joshi J, Xu B, Rubart M, Chang Y, Bao X, Chaliki HP, et al. Optogenetic Control of Engrafted Human Induced Pluripotent Stem Cell-Derived Cardiomyocytes in Live Mice: A Proof-of-Concept Study. *Cells.* 2022;11(6).
81. John J. Dziak DLC, Runze Li, Kaylee Litson, Yajnaseni Chakraborti. tvem: Time-Varying Effect Models. https://cran.r-project.org/web/packages/tvem/index.html. Accessed April 8, 2024.

FIGURES

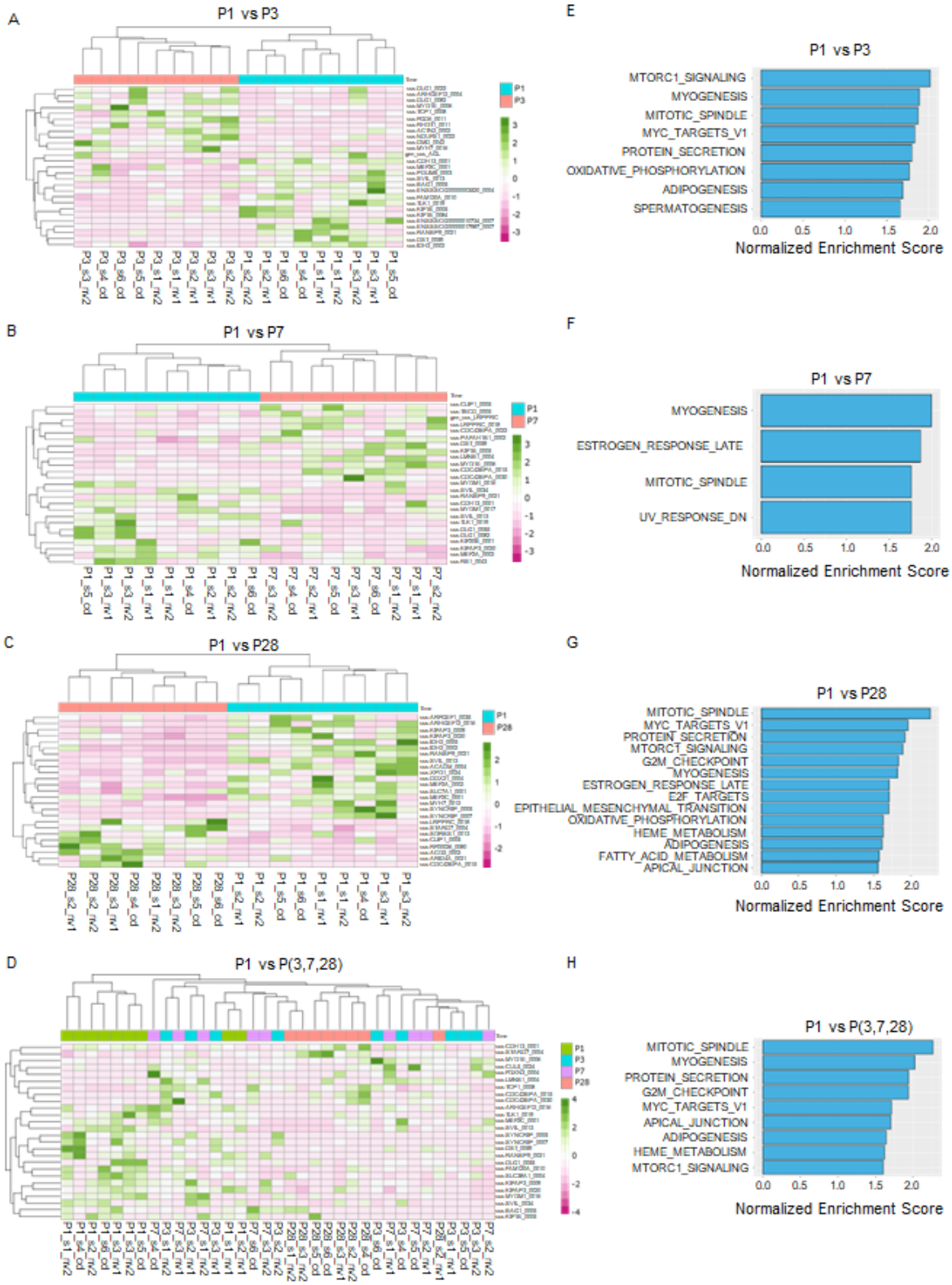
A
P1 vs P3
B
P1 vs P7
C
P1 vs P28
D
P1 vs P(3,7,28)
E
P1 vs P3
MTORC1_SIGNALING
MYOGENESIS
MITOTIC_SPINDLE
MYC_TARGETS_V1
PROTEIN_SECRETION
OXIDATIVE_PHOSPHORYLATION
ADIPOGENESIS
SPERMATOGENESIS
0.0 0.5 1.0 1.5 2.0
Normalized Enrichment Score
F
P1 vs P7
MYOGENESIS
ESTROGEN_RESPONSE_LATE
MITOTIC_SPINDLE
UV_RESPONSE_DN
0.0 0.5 1.0 1.5 2.0
Normalized Enrichment Score
G
P1 vs P28
MITOTIC_SPINDLE
MYC_TARGETS_V1
PROTEIN_SECRETION
MTORC1_SIGNALING
G2M_CHECKPOINT
MYOGENESIS
ESTROGEN_RESPONSE_LATE
E2F_TARGETS
EPITHELIAL_MESENCHYMAL_TRANSITION
OXIDATIVE_PHOSPHORYLATION
HEME_METABOLISM
ADIPOGENESIS
FATTY_ACID_METABOLISM
APICAL_JUNCTION
0.0 0.5 1.0 1.5 2.0
Normalized Enrichment Score
H
P1 vs P(3,7,28)
MITOTIC_SPINDLE
MYOGENESIS
PROTEIN_SECRETION
G2M_CHECKPOINT
MYC_TARGETS_V1
APICAL_JUNCTION
ADIPOGENESIS
HEME_METABOLISM
MTORC1_SIGNALING
0.0 0.5 1.0 1.5 2.0
Normalized Enrichment Score

Figure 1. Differentially expressed circRNAs in neonatal pig hearts and functional enrichment analysis. (A-D) A heatmap of differentially expressed and cell cycle related circRNAs depicting expression patterns from various comparisons including P1 versus P3 **(A**), P1 versus P7 **(B)**, P1 versus P28 **(C)**, and P1 versus P3, P7, and P28 **(D)**. circRNAs with high expression values are colored in dark green while those with low expression values are in dark pink. **(E-H**) Pathway enrichment analysis plots of top ranked cell cycle-related hallmark pathways from various comparisons including **(E)** P1 versus P3, **(F)** P1 versus P7, **(G)** P1 versus P28, and **(H)** P1 versus P3, P7, and P28. Panels A-H were generated using circRNA data from 35 batch corrected RNA samples obtained from 24 pig hearts sequenced by CD Genomics Inc. (“cd”), and Novogene Inc. (“nv1” and “nv2”).

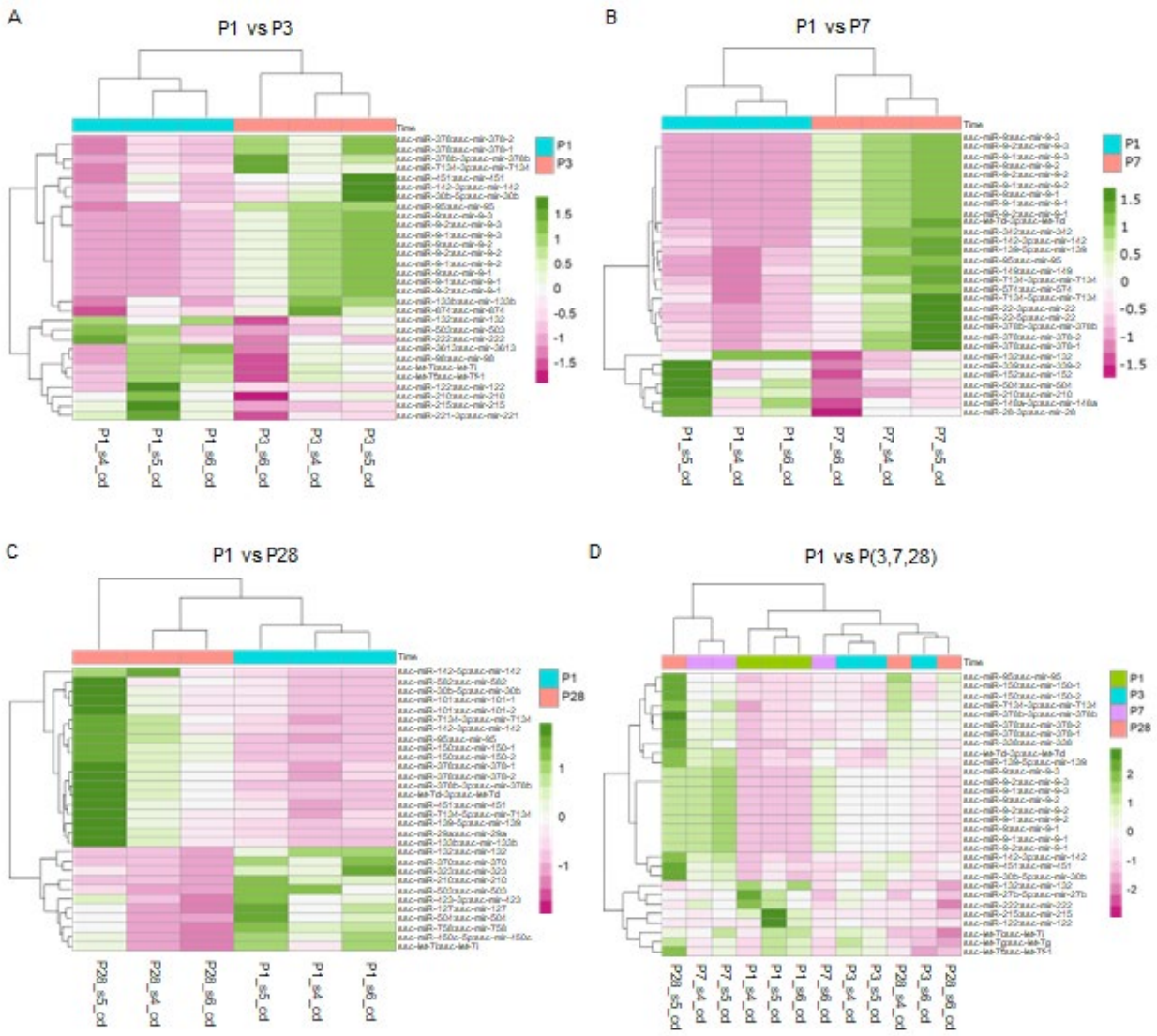

Figure 2. Differentially expressed miRNAs in neonatal pig hearts and functional enrichment analysis. (A-D) A heatmap of top 30 differentially expressed miRNAs depicting expression time specific patterns at different experimental designs including **(A)** P1 versus P3, **(B)** P1 versus P7, **(C)** P1 versus P28, and **(D)** P1 versus P3, P7, and P28. circRNAs with high expression values are colored in dark green while those with low expression values are colored in dark pink. The heatmap plots displayed indicate noticeable differences in expression patterns (either higher or lower) at P1 compared to the other days, suggesting a significant alteration in the expression of miRNAs during the

postnatal development of pig hearts. All panels were generated using miRNA data from 12 RNA samples obtained from 12 pig hearts at different postnatal days (P1, P3, P7, and P28).

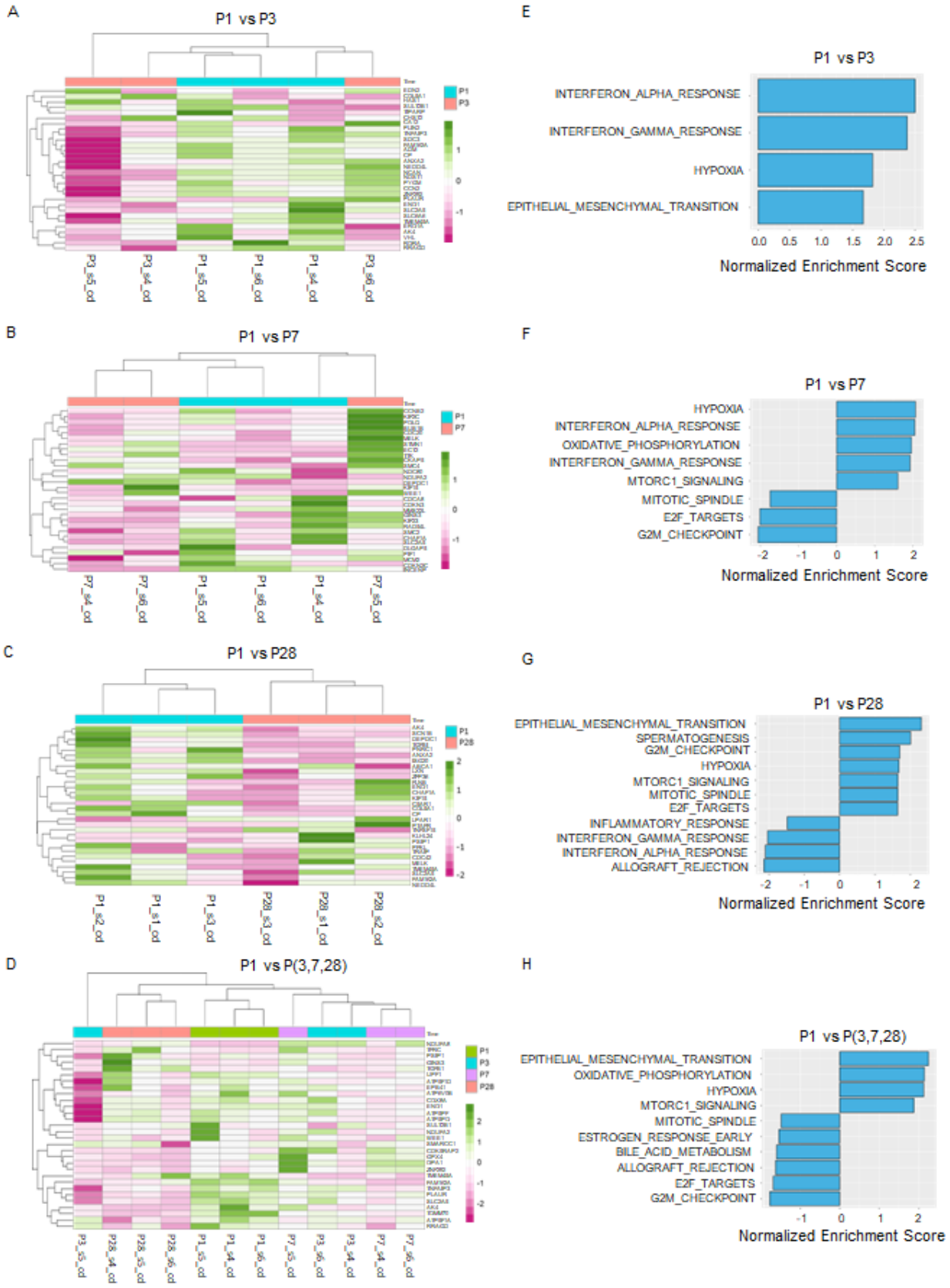
A
P1 vs P3
P3_s5_cd
P3_s4_cd
P1_s5_cd
P1_s6_cd
P1_s4_cd
P3_s6_cd
B
P1 vs P7
P7_s4_cd
P7_s6_cd
P1_s5_cd
P1_s6_cd
P1_s4_cd
P7_s5_cd
C
P1 vs P28
P1_s2_cd
P1_s1_cd
P1_s3_cd
P28_s3_cd
P28_s1_cd
P28_s2_cd
D
P1 vs P(3,7,28)
P3_s5_cd
P28_s4_cd
P28_s5_cd
P28_s6_cd
P1_s5_cd
P1_s4_cd
P1_s6_cd
P7_s5_cd
P3_s6_cd
P3_s4_cd
P7_s4_cd
P7_s6_cd
E
P1 vs P3
INTERFERON_ALPHA_RESPONSE
INTERFERON_GAMMA_RESPONSE
HYPOXIA
EPITHELIAL_MESENCHYMAL_TRANSITION
Normalized Enrichment Score
F
P1 vs P7
HYPOXIA
INTERFERON_ALPHA_RESPONSE
OXIDATIVE_PHOSPHORYLATION
INTERFERON_GAMMA_RESPONSE
MTORC1_SIGNALING
MITOTIC_SPINDLE
E2F_TARGETS
G2M_CHECKPOINT
Normalized Enrichment Score
G
P1 vs P28
EPITHELIAL_MESENCHYMAL_TRANSITION
SPERMATOGENESIS
G2M_CHECKPOINT
HYPOXIA
MTORC1_SIGNALING
MITOTIC_SPINDLE
E2F_TARGETS
INFLAMMATORY_RESPONSE
INTERFERON_GAMMA_RESPONSE
INTERFERON_ALPHA_RESPONSE
ALLOGRAFT_REJECTION
Normalized Enrichment Score
H
P1 vs P(3,7,28)
EPITHELIAL_MESENCHYMAL_TRANSITION
OXIDATIVE_PHOSPHORYLATION
HYPOXIA
MTORC1_SIGNALING
MITOTIC_SPINDLE
ESTROGEN_RESPONSE_EARLY
BILE_ACID_METABOLISM
ALLOGRAFT_REJECTION
E2F_TARGETS
G2M_CHECKPOINT
Normalized Enrichment Score

1

Figure 3. Differentially expressed mRNAs in neonatal pig hearts and functional enrichment analysis. (A-D) A heatmap of top 30 differentially expressed and cell cycle related mRNAs depicting expression patterns from various comparisons including **(A)** P1 versus P3, **(B)** P1 versus P7, **(C)** P1 versus P28, and **(D)** P1 versus P3, P7, and P28. mRNAs with high expression values are colored in dark green while those with low expression values are in dark pink. **(E-H)** Pathway enrichment analysis plots of significantly enriched hallmark pathways from various comparisons including **(E)** P1 versus P3, **(F)** P1 versus P7, **(G)** P1 versus P28, and **(H)** P1 versus P3, P7, and P28. Pathways significantly enriched (FDR < 0.05) are colored in green. All panels were generated using miRNA data from 12 RNA samples obtained from 12 pig hearts at different postnatal days (P1, P3, P7, and P28).

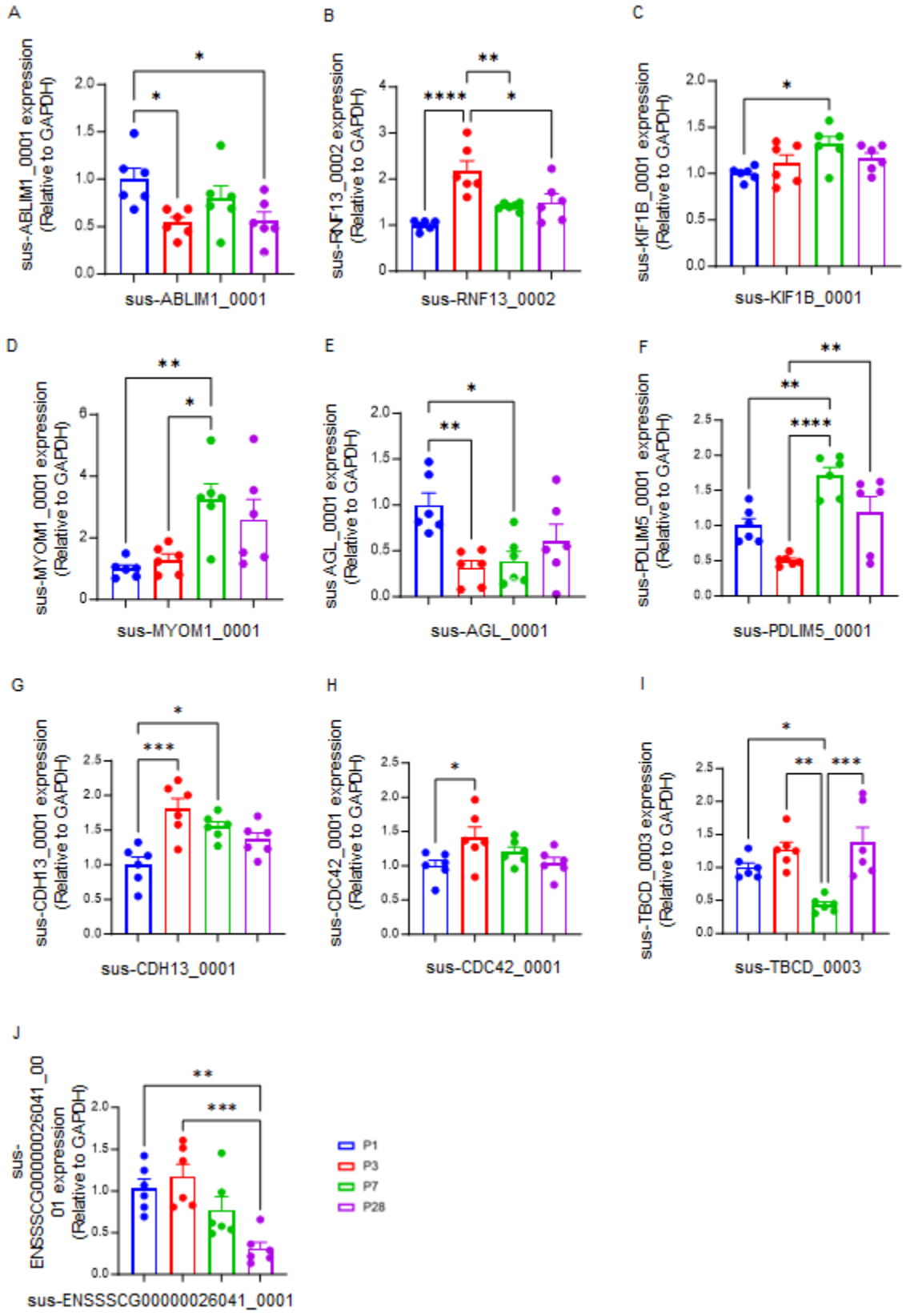
A
sus-ABLIM1_0001 expression (Relative to GAPDH)
sus-ABLIM1_0001
B
sus-RNF13_0002 expression (Relative to GAPDH)
sus-RNF13_0002
C
sus-KIF1B_0001 expression (Relative to GAPDH)
sus-KIF1B_0001
D
sus-MYOM1_0001 expression (Relative to GAPDH)
sus-MYOM1_0001
E
sus AGL_0001 expression (Relative to GAPDH)
sus-AGL_0001
F
sus-PDLIM5_0001 expression (Relative to GAPDH)
sus-PDLIM5_0001
G
sus-CDH13_0001 expression (Relative to GAPDH)
sus-CDH13_0001
H
sus-CDC42_0001 expression (Relative to GAPDH)
sus-CDC42_0001
I
sus-TBCD_0003 expression (Relative to GAPDH)
sus-TBCD_0003
J
sus-ENSSSCG00000026041_0001 expression (Relative to GAPDH)
sus-ENSSSCG00000026041_0001
P1
P3
P7
P28

1

Figure 4. Validation of circRNA expression in neonatal pig hearts. (A-J) qRT-PCR was performed to validate the expression of ten selected circRNAs associated with the cell cycle regulation pathway in neonatal pig hearts. All data were presented as mean ± SEM. Statistical comparisons between two groups in multi groups were evaluated by one-way ANOVA with Tukey's Honestly Significant Difference Test for panels A-J. n=6 pig hearts for each group. *p<0.05, **p<0.01, ***p<0.001, and ****p<0.0001 when comparing the expression levels between them. The relative expression levels of circRNAs were normalized to GAPDH reference gene.

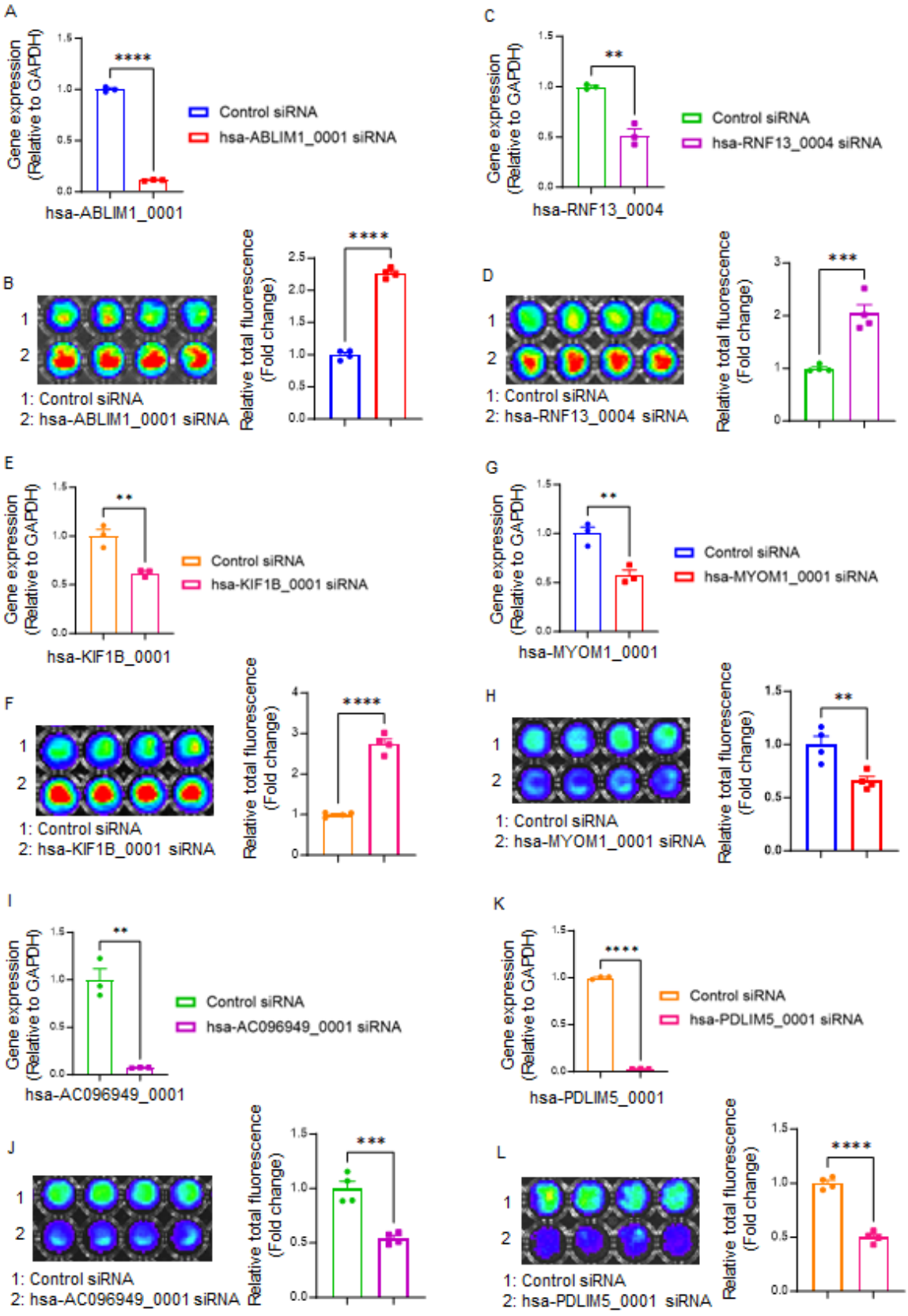
A
Gene expression (Relative to GAPDH)
****
Control siRNA
hsa-ABLIM1_0001 siRNA
hsa-ABLIM1_0001
B
1
2
1: Control siRNA
2: hsa-ABLIM1_0001 siRNA
Relative total fluorescence (Fold change)
****
C
Gene expression (Relative to GAPDH)
**
Control siRNA
hsa-RNF13_0004 siRNA
hsa-RNF13_0004
D
1
2
1: Control siRNA
2: hsa-RNF13_0004 siRNA
Relative total fluorescence (Fold change)
***
E
Gene expression (Relative to GAPDH)
**
Control siRNA
hsa-KIF1B_0001 siRNA
hsa-KIF1B_0001
F
1
2
1: Control siRNA
2: hsa-KIF1B_0001 siRNA
Relative total fluorescence (Fold change)
****
G
Gene expression (Relative to GAPDH)
**
Control siRNA
hsa-MYOM1_0001 siRNA
hsa-MYOM1_0001
H
1
2
1: Control siRNA
2: hsa-MYOM1_0001 siRNA
Relative total fluorescence (Fold change)
**
I
Gene expression (Relative to GAPDH)
**
Control siRNA
hsa-AC096949_0001 siRNA
hsa-AC096949_0001
J
1
2
1: Control siRNA
2: hsa-AC096949_0001 siRNA
Relative total fluorescence (Fold change)
***
K
Gene expression (Relative to GAPDH)
****
Control siRNA
hsa-PDLIM5_0001 siRNA
hsa-PDLIM5_0001
L
1
2
1: Control siRNA
2: hsa-PDLIM5_0001 siRNA
Relative total fluorescence (Fold change)
****

1

Figure 5. circRNAs that modulate cardiomyocyte cell cycle. hiPSC-CMs at day 28 after initiation of cardiac differentiation were utilized. The efficiency of siRNA-based knockdown of circRNAs in hiPSC-CMs was determined by qRT-PCR. The relative expression levels of circRNAs were normalized to GAPDH reference gene. Cell number was evaluated by bioluminescence analysis. Data were presented as percentage. **(A, C, E, G, I,** and **K)** Evaluation of the expression of hsa-ABLIM1_0001, hsa-RNF13_0004, hsa-KIF1B_0001, has-MYOM1_0001, has-AC096949_0001, and has-PDLIM5_0001 in hiPSC-CMs after siRNA treatment. **(B, D, F, H, J,** and **L)** Bioluminescence assay and quantification of bioluminescent signal intensity in hiPSC-CMs with siRNA-based knock down of the specific circRNAs. All data were presented as mean ± SEM. Statistical analysis was performed via student's t-test. n=3 technical replicates in each group for panels **A, C, E, G, I,** and **K**. n=4 technical replicates in each group for panels **B, D, F, H, J,** and **L**. **p<0.01, ***p<0.001, and ****p<0.0001.

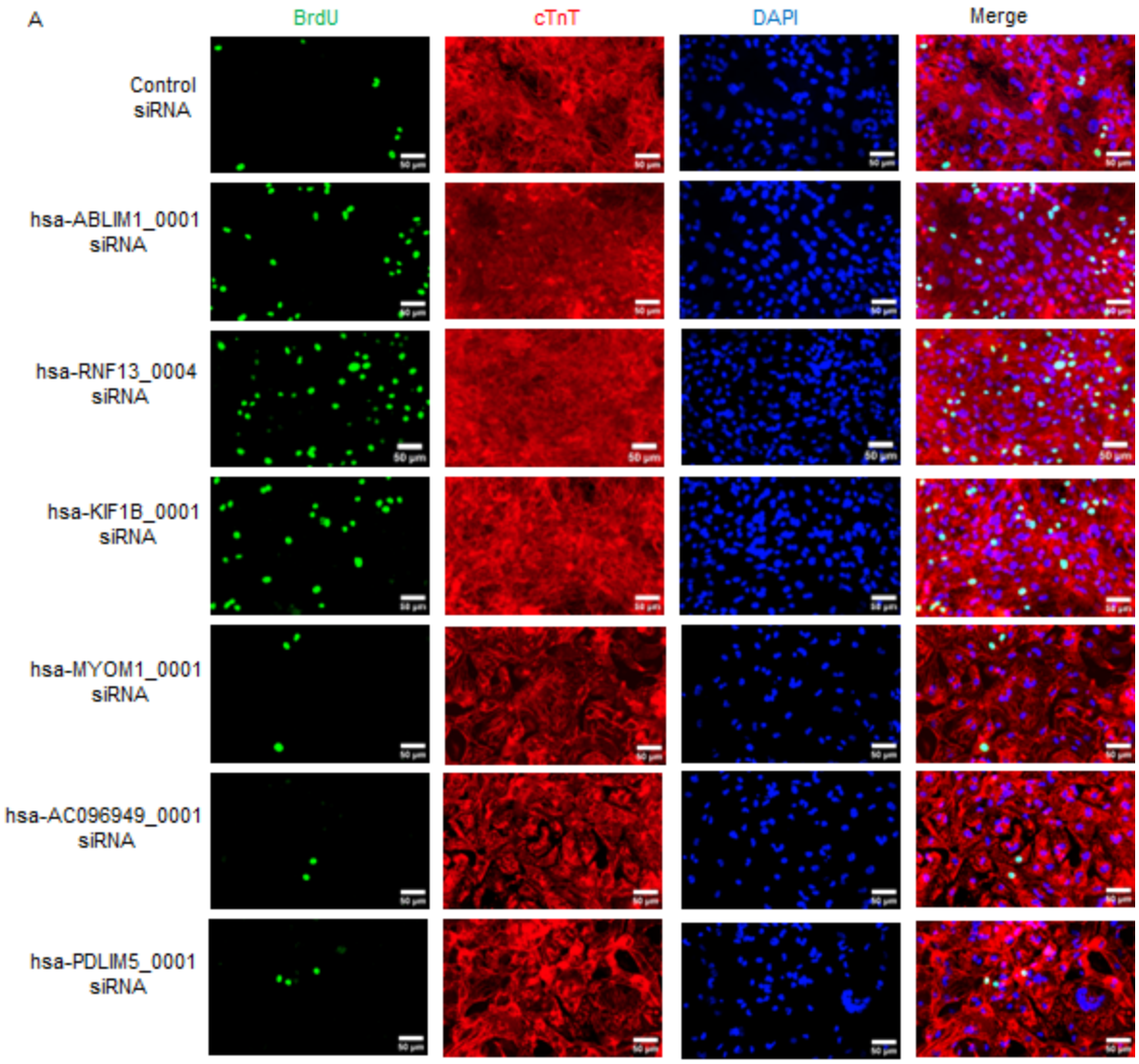
A
BrdU
cTnT
DAPI
Merge
Control siRNA
hsa-ABLIM1_0001 siRNA
hsa-RNF13_0004 siRNA
hsa-KIF1B_0001 siRNA
hsa-MYOM1_0001 siRNA
hsa-AC096949_0001 siRNA
hsa-PDLIM5_0001 siRNA
B
BrdU+ cardiomyocyte nuclei (%)
0
5
10
15
20
25
**
****
***
****
****
****
CON siRNA
hsa-ABLIM1_0001 siRNA
hsa-RNF13_0004 siRNA
hsa-KIF1B_0001 siRNA
hsa-MYOM1_0001 siRNA
hsa-AC096949_0001 siRNA
hsa-PDLIM5_0001 siRNA

1

Figure 6. Evaluation of cardiomyocyte cell cycle via Bromodeoxyuridine (BrdU) incorporation assay. hiPSC-CMs at day 28 after initiation of cardiac differentiation were used. Cell cycle was assessed by immunostaining using antibodies against BrdU (to label cells in S phase). Cardiomyocytes were labeled using anti-human cTnT immunostaining, all nuclei were counterstained with DAPI. The prevalence of BrdU positively stained nuclei of hiPSC-CMs was counted and normalized to the total number of cardiomyocyte nuclei. Data were presented as percentage. **(A)** Representative images of anti-BrdU immunostaining in hiPSC-CMs. (B) Quantification of the prevalence of BrdU positively stained nuclei of hiPSC-CMs after siRNA-based knock down. All data were presented as mean ± SEM. Statistical analysis was performed via one-way ANOVA with Tukey's Honestly Significant Difference test. n= 30 technical replicates in each group. **p<0.01, ***p<0.001, and ****p<0.0001.

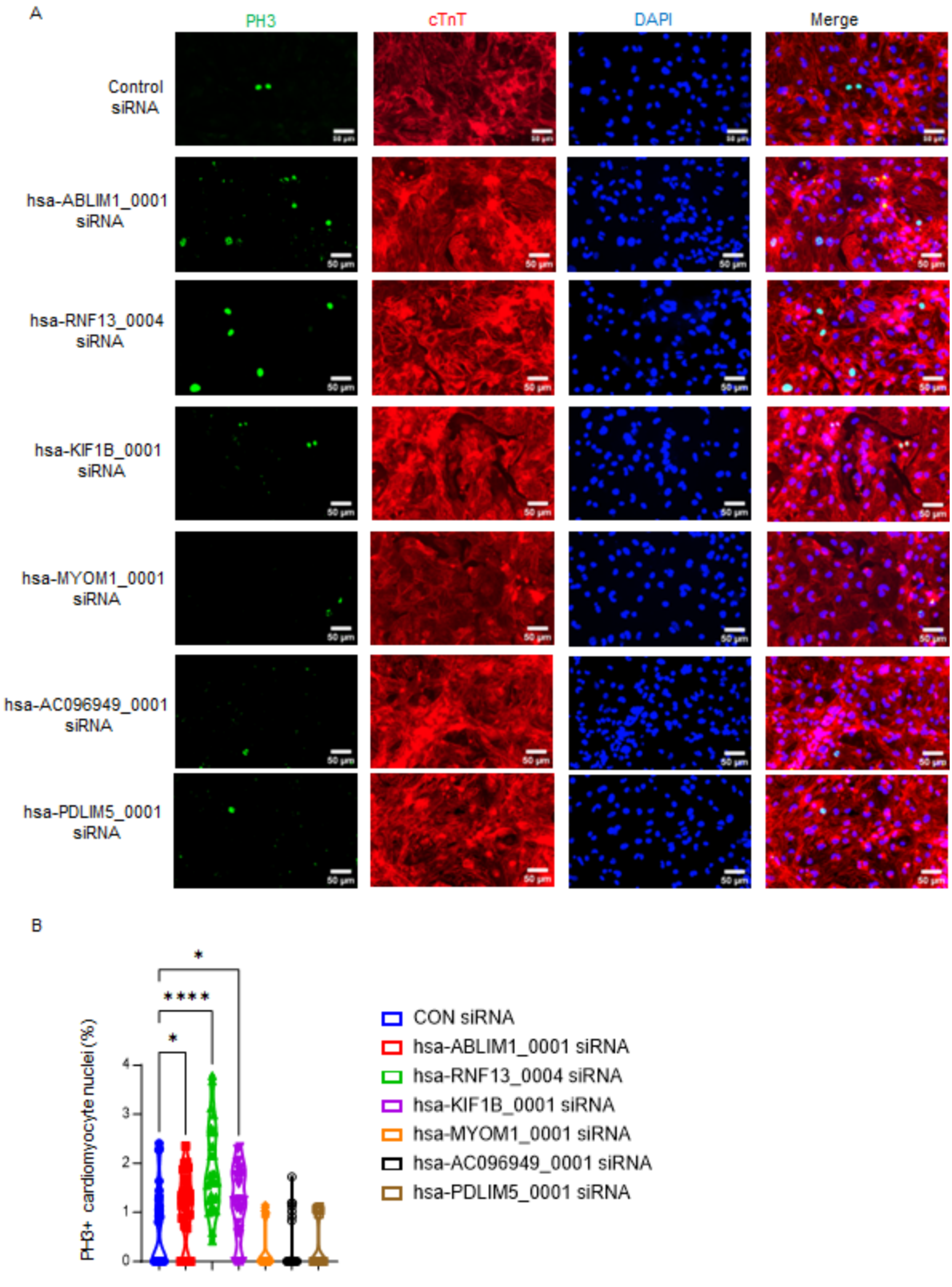
A
PH3
cTnT
DAPI
Merge
Control siRNA
hsa-ABLIM1_0001 siRNA
hsa-RNF13_0004 siRNA
hsa-KIF1B_0001 siRNA
hsa-MYOM1_0001 siRNA
hsa-AC096949_0001 siRNA
hsa-PDLIM5_0001 siRNA
B
PH3+ cardiomyocyte nuclei (%)
0
1
2
3
4
*
****
*
CON siRNA
hsa-ABLIM1_0001 siRNA
hsa-RNF13_0004 siRNA
hsa-KIF1B_0001 siRNA
hsa-MYOM1_0001 siRNA
hsa-AC096949_0001 siRNA
hsa-PDLIM5_0001 siRNA

1

Figure 7. Evaluation of cardiomyocyte cell cycle via immunostaining for phosphorylated histone H3 (PH3). Cell cycle was assessed by immunostaining using antibodies against PH3 (to label cells in mitosis phase). Cardiomyocytes were labeled using anti-human cTnT immunostaining, all nuclei were counterstained with DAPI. The prevalence of PH3 positively stained nuclei of hiPSC-CMs was counted and normalized to the total number of cardiomyocyte nuclei. Data were presented as percentage. **(A)** Representative images of anti-PH3 immunostaining in hiPSC-CMs. (B) Quantification of the prevalence of PH3 positively stained nuclei of hiPSC-CMs after siRNA-based knock down. All data were presented as mean ± SEM. Statistical analysis was performed via one-way ANOVA with Tukey's Honestly Significant Difference test. n= 30 technical replicates in each group. *p<0.05, and ****p<0.0001.

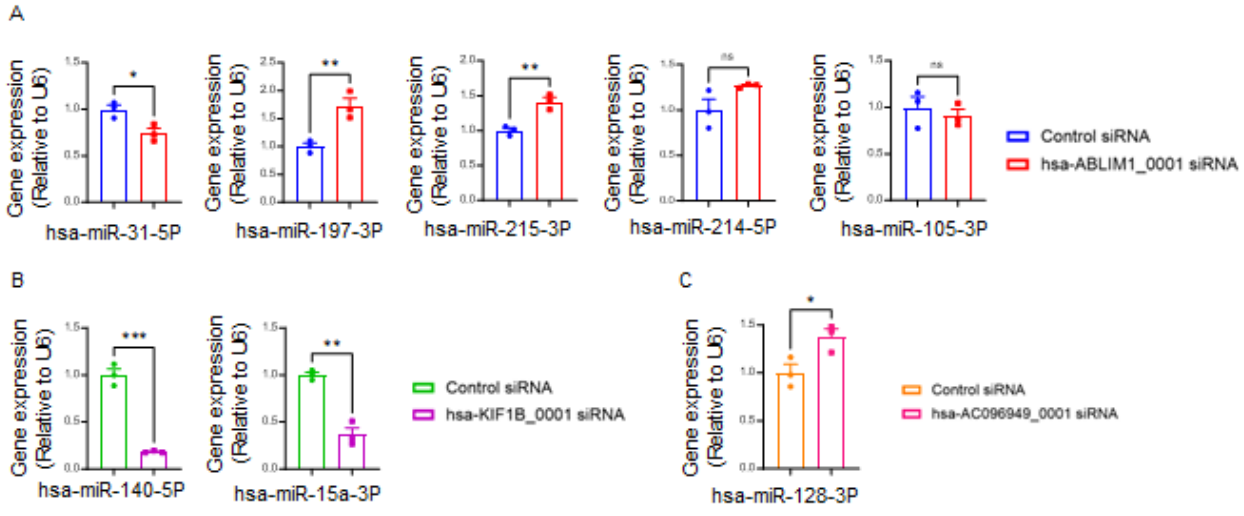

Figure 8. Impact of circRNA knockdown on the expression of miRNAs. hiPSC-CMs at day 28 after the initiation of cardiac differentiation were used. qRT-PCR was used to evaluate the expression level of various miRNAs in hiPSC-CMs. This included the evaluation of hsa-miR-31-5P, hsa-miR-197-3P, hsa-miR-215-3P, hsa-miR-214-5P and

hsa-miR-105-3P in hiPSC-CMs treated with hsa-ABLIM1_0001 siRNA **(A)**, hsa-miR-140-5P and hsa-miR-15a-3P in hiPSC-CMs treated with hsa-KIF1B_0001 siRNA **(B)**, and hsa-miR-128-3P in hiPSC-CMs treated with hsa-AC096949_0001 siRNA **(C)**. The relative expression levels of miRNAs were normalized to U6 reference gene. All data were presented as mean ± SEM. Statistical analysis was performed via the Student's t-test. n=3 technical replicates in each group. *p<0.05, **p<0.01, and ***p<0.001.